Response of the East Antarctic Ice Sheet to past and future climate change

Response of the East Antarctic Ice Sheet to Past and Future Climate Change

Chris R. Stokes[1*], Nerilie J. Abram[2,3], Michael J. Bentley[1], Tamsin L. Edwards[4], Matthew H. England[5,6], Annie Foppert[7] , Stewart S.R. Jamieson[1], Richard S. Jones[8,9], Matt A. King[10,11,], Jan T.M. Lenaerts[12], Brooke Medley[13], Bertie W.J. Miles[1], Guy J.G. Paxman[14], Catherine Ritz[15], Tina van de Flierdt[16], Pippa L. Whitehouse[1]

[1]Department of Geography, Durham University, UK
[2]Research School of Earth Sciences, Australian National University, Canberra ACT 2601, Australia
[3]Australian Centre for Excellence in Antarctic Science, Australian National University, Canberra ACT 2601, Australia
[4]Department of Geography, King's College London, UK
[5]Climate Change Research Centre, University of New South Wales, Australia
[6]Australian Centre for Excellence in Antarctic Science, University of New South Wales, Sydney NSW, Australia
[7]Australian Antarctic Program Partnership, Institute for Marine and Antarctic Studies, University of Tasmania, Hobart, Australia
[8]School of Earth, Atmosphere and Environment, Monash University, Clayton, Victoria, Australia
[9]Securing Antarctica's Environmental Future, Monash University, Clayton, Victoria, Australia
[10]School of Geography, Planning, and Spatial Sciences, University of Tasmania, Australia
[11]Australian Centre for Excellence in Antarctic Science, University of Tasmania, Hobart TAS 7001, Australia
[12]Department of Atmospheric and Oceanic Sciences, University of Colorado Boulder, USA
[13]Cryospheric Sciences Laboratory, NASA Goddard Space Flight Center, USA
[14]Lamont-Doherty Earth Observatory, Columbia University, USA
[15]Institut des Géosciences de l'Environnement, Université Grenoble Alpes, France
[16]Department of Earth Science and Engineering, Imperial College London, UK

*Corresponding author: Chris R Stokes (c.r.stokes@durham.ac.uk)

Preface: The East Antarctic Ice Sheet (EAIS) contains the vast majority of Earth's glacier ice (~52 metres sea-level equivalent), but is often viewed as less vulnerable to global warming than the West Antarctic or Greenland ice sheets. However, some regions of the EAIS have lost mass over recent decades, prompting the need to re-evaluate its sensitivity to climate change. Here we review the EAIS's response to past warm periods, synthesise current observations of change, and evaluate future projections. Some marine-based catchments that underwent significant mass loss during past warm periods are currently losing mass, but most projections indicate increased accumulation across the EAIS over the 21st Century, keeping the ice sheet broadly in balance. Beyond 2100, high emissions scenarios generate increased ice discharge and potentially several metres of sea-level rise within just a few centuries, but substantial mass loss could be averted if the Paris Agreement to limit warming below 2°C is satisfied.

1. Introduction

Over recent decades, ice loss from Antarctica has exceeded mass gains and its contribution to sea-level rise has accelerated[1-9]. The largest imbalances are found in the West Antarctic Ice Sheet (WAIS: Fig. 1d), which holds 5.3 m sea-level equivalent (SLE)[10] and lost over 2,000 Gt of ice between 1992 and 2017, adding ~6 mm to global mean sea level[1]. This imbalance is attributed to warm ocean currents - modified Circumpolar Deep Water (CDW) - melting the underside of floating ice shelves, causing marginal ice thinning, grounding line retreat and increased ice discharge[11-18]. Furthermore, the WAIS is marine-based, resting on topography below sea level that deepens inland (Fig. 1e)[10]. In the absence of buttressing ice shelves[16], retreat could rapidly propagate inland via a feedback known as 'Marine Ice Sheet Instability'[19].

The vulnerability of the WAIS was first recognised in the 1970s[20], prompting a huge growth in research[21]. In comparison, much less work has focussed on the vulnerability of the East Antarctic Ice Sheet (EAIS), which is an order of magnitude larger (52.2 m SLE)[10] and generally viewed as less sensitive to ocean-climate warming. This view stems from the fact that large parts of the EAIS have persisted for millions of years[22], recent mass balance estimates tend towards equilibrium or show modest mass gains[1,2,5,23,24] (Fig. 2), and most model projections show low sensitivity to climate change over the next century[25]. However, some recent observations suggest the EAIS may be more sensitive than previously thought. Although uncertainties are large and often obscure even the sign of any change, the latest efforts to reconcile its mass balance from multiple methods[1,2] have raised the possibility of overall mass loss since ~2014 (Fig. 2). Furthermore, numerous studies[4,5,6,8], including those reporting overall mass gain[7,9,23,24], detect clear signals of regional mass loss from some marine-based catchments (e.g. Wilkes Land: Fig. 1e). Like the WAIS, mass loss has been attributed to modified CDW proximal to major outlet glaciers[4,26-30] that may also be susceptible to Marine Ice Sheet Instability[10,31], driving ice sheet thinning[5,7,11,32], grounding line retreat[17,33-35], and the retreat[30,36] and disintegration[37,38] of floating ice tongues/shelves.

Of further concern is that marine-based sectors of the EAIS lost mass during past warm periods[39-42] and some numerical modelling predicts significant sea-level contributions from them over the coming centuries[31,43-46]. In contrast, 'terrestrial' regions of the EAIS, grounded on land well above sea level, are gaining mass through increased accumulation (e.g. Dronning Maud Land: Fig. 1e), albeit with large inter-annual variability[5-9,47,48]. A key issue is that observational time-series of accumulation or ice discharge are generally too short to elucidate whether recent trends are significant or represent natural variability in the ocean-climate system[49-51], prompting a question of huge scientific and societal importance: what will happen to the East Antarctic Ice Sheet? With an emphasis on marine-based versus terrestrial sectors, we address this question by reviewing how the EAIS changed during past warm periods and

during deglaciation from the Last Glacial Maximum; synthesise current observations of change; and then evaluate future projections through to 2500.

2. Response to Past Warm Periods

Since widespread glaciation of Antarctica at the Eocene-Oligocene Transition[52] (34–33.5 Ma: Fig. 1g), climatic changes have caused substantial advance and retreat of the EAIS[53,54]. Early to Mid-Miocene (24–14 Ma) sediment records in the Ross Sea, for example, provide evidence for multiple orbitally-paced fluctuations in EAIS extent[55,56], recorded by erosional hiatuses representing expansion[57], and sediment provenance and vegetation changes indicating parts of East Antarctica were ice-free[58,59].

The largest reduction in EAIS volume during the past 20 million years occurred during the Mid-Miocene Climatic Optimum (17.0–14.8 Ma), when average atmospheric CO_2 concentrations were around 600–800 ppm (ranging from 300–1400 ppm)[60] and sea surface temperatures peaked at ~11–17°C off the Adélie Coast[61] and ~6–10 °C in the Ross Sea[56]. Under these conditions, ice sheet modelling[57] can simulate tens of metres of SLE contribution from East Antarctica, with mass loss focussed in the three main subglacial basins: the Aurora (ASB), Wilkes (WSB) and Recovery (RSB) (Fig. 1a). Terrestrial sectors are also likely to have retreated, but recent sediment provenance analysis from the central Ross Sea[62] reveals that far-field sea-level records[63] can be reconciled without substantial loss of terrestrial ice in East Antarctica, consistent with coupled climate and ice sheet modeling[57]. Notably, average Mid-Miocene CO_2 concentrations could be reached by 2100[64]; although orbital forcing was stronger than present and global atmospheric temperatures (7–8°C)[65] were significantly warmer than projected for 2100.

The most recent epoch when atmospheric CO_2 concentrations last exceeded 400 ppm was the Pliocene (5.33–2.58 Ma)[66]. Mid-Pliocene (~3.3–3.0 Ma) atmospheric temperatures were ~2–4°C warmer than present[67] and global mean sea level was around 10–25 m higher[68-71]. Given the combined volume of the WAIS and Greenland Ice Sheet (~12 m), and that their mid-Pliocene minima were likely asynchronous[72], most sea-level estimates require an EAIS contribution[21,54,71].

Early work on the EAIS response to mid-Pliocene warming focussed on marine diatoms in subglacial diamictites of the Sirius Group in the Transantarctic Mountains[22,73]. Ambiguity regarding the transport mechanism of these diatoms made it difficult to locate which regions lost mass, but recent work[74] supports at least partial retreat of both the ASB and WSB. Marine sediment records provide more direct evidence of substantial retreat of the WSB, inferred from a shift in the provenance of fine-grained detrital sediment[39], contemporaneous

with a shift in marine productivity, indicating a reduction in local sea-ice coverage[75] and a southward migration of the Southern Ocean Polar Front[76]. Substantial retreat of the ASB is also inferred from records of ice-rafted debris[40,77], and from erosional signatures beneath the catchment of Totten Glacier, which could have contributed over 2 m SLE[78]. Elsewhere, evidence of elevated fjord temperatures and vegetated landscapes in the Transantarctic Mountains suggests significant retreat of marine-terminating glaciers[79]; and the Lambert Glacier-Amery Ice Shelf system was highly sensitive to Southern Ocean warming[80].

In contrast, mid-Pliocene retreat of terrestrial sectors of the EAIS and/or the RSB is largely unknown, due to a lack of empirical evidence. Some ice sheet modelling is able to simulate retreat and thinning of the RSB[44,46,81], alongside the WSB and ASB (Fig. 1b), but it has generally proved challenging to simulate mid-Pliocene retreat of marine-based sectors[54,82]. The amount of modelled retreat is sensitive to assumed pre-Pliocene ice sheet configurations[81], climate model forcing[83], and ice sheet model parameters[84], with those simulating the most retreat (e.g. Fig. 1b) often requiring additional processes to enhance mass loss[44,54,81,85], some of which are debated (e.g. Marine Ice-Cliff Instability, discussed below)[86].

Marine-based sectors were also vulnerable during the warmest interglacials of the Pleistocene (2.58–0.017 Ma), with offshore evidence of mass loss in the WSB[41]. During Marine Isotope Stage 11 (~400 ka), subglacial precipitates of opal and calcite[42] suggest the ice margin was ~700 km inland of its current position, potentially contributing ~3–4 m SLE when global atmospheric temperatures were only 1–2°C warmer than present. Terrestrial records from the Transantarctic Mountains[87] also indicate ice surface elevation fluctuations of hundreds of metres during the Pleistocene, similar in magnitude to those during the Pliocene.

Mass loss during the last interglacial (Marine Isotope Stage 5: ~130–115 ka) is equivocal[21]. Ice cores and glacio-isostatic adjustment modelling[88] suggest ice-surface lowering is plausible in the WSB and ASB, with other work[89] placing an upper sea-level contribution of 0.4–0.8 m from the WSB. Sea-level records[71] require no more than a few metres from Antarctica, which is more likely from the WAIS, but the EAIS cannot currently be ruled out.

3. The Last Deglaciation

During the Last Glacial Maximum (27–20 ka), marine-based sectors of the EAIS expanded to near the continental shelf edge[90] (Fig. 1c). Evidence of ice margin extent and subsequent retreat is only available from some regions, but typically indicates deglaciation commencing at ~19–18 ka (e.g. the Lambert-Amery system), with grounding lines reaching the mid-continental shelf in some locations at ~15 ka (e.g. Ross Sea sector)[90-92]. The maximum extent

in the Weddell Sea sector is less clear[93], with recent evidence[94] of an oscillating grounding line position on the outer continental shelf until ~12 ka. A rapid rise in global sea level occurred at ~14.6 ka (Meltwater Pulse 1a), but Antarctica's contribution was limited (≤1.3 m)[95]; with little direct evidence (e.g. ice surface elevation changes) for substantial changes in EAIS geometry[90,92,93], although increased ice-rafted debris is recorded in the vicinity of the Weddell Sea[96].

Most regions of the EAIS had retreated prior to the Holocene (~11.7 ka), but some experienced a delayed response (e.g. Adélie Basin, Mac. Robertson Land, Prydz Bay)[90], or even slightly thickened and advanced during deglaciation (e.g. Transantarctic Mountains)[97,98]. Furthermore, data from the Lambert-Amery system and Transantarctic Mountains indicate most ice surface lowering occurred during the Early-Mid Holocene, continuing in some locations into the last few millennia[99-101].

Bed topography influenced the retreat of marine-based sectors across the inner-continental shelf[91,102,103] and may explain some regional asynchronicity. Geomorphological evidence on the sea-floor of the Mertz Trough, Prydz Channel and western Ross Sea, for example, indicates marked accelerations in grounding line retreat across over-deepened basins[90,91,104]. Rapid retreat across over-deepenings in the Ross Sea was also associated with hundreds of metres of ice surface lowering over several centuries[99,101]. In contrast, retreat was slowed by elevated bed topography[102]. Isostatic rebound in the Weddell and Ross Seas may also have exerted a stabilising effect[105], but this process has not been explored elsewhere in East Antarctica.

Ice sheet modelling indicates the greatest ice losses occurred in the major marine embayments during deglaciation (e.g. Ross Sea, Weddell Sea and, to a lesser degree, Prydz Bay), with mass loss elsewhere varying in both magnitude and timing depending on the model[106-108]. Initial retreat was likely triggered by a combination of ocean, atmosphere and sea-level changes[21]. In at least the Ross Sea, atmospheric conditions controlled the timing and spatial pattern of early deglaciation[109]. Meanwhile, terrestrial sectors of the interior EAIS, and areas of the Transantarctic Mountains, likely thickened due to increased snowfall following the Last Glacial Maximum[97,106]. Oceanic warming became an increasingly important control on marine-based retreat during deglaciation[90], driving a positive feedback whereby ice loss freshened surface ocean waters, possibly reducing the formation of dense Antarctic bottom waters, and facilitating incursions of modified CDW onto the continental shelf[108]. Holocene ice loss in the Ross Sea, for example, corresponds with ocean warming and the development of ice shelf cavities and modified CDW intrusion[102,109].

Palaeo-data of grounding line retreat and ice sheet thinning during deglaciation provide important context for modern-day observations (Fig. 3). The highest rates of grounding line retreat exceeded 100 m yr^{-1}, possibly up to 800 m yr^{-1} (Fig. 3a). Deglacial thinning rates from the flanks of outlet glaciers were typically 0.06–0.76 m yr^{-1}, possibly up to several metres per year (Fig. 3c). These time-averaged rates were sustained over several centuries and may mask more extreme rates, but reveal that some present-day thinning (>1 m yr^{-1}) and retreat rates (>200 m yr^{-1}) are comparable to the last deglaciation.

4. Recent Ocean Conditions and Ice Dynamics

Evidence and modelling from past warm periods clearly points to the enhanced sensitivity of East Antarctica's three major marine basins (RSB, WSB, ASB). Terrestrial regions respond mainly to atmospheric forcing, but these marine-based sectors respond to both atmospheric and oceanic processes, potentially involving Marine Ice Sheet Instability. Hence, ocean conditions and bathymetry on the continental shelf are important to understand in relation to EAIS dynamics.

Around most of East Antarctica, strong easterly winds drive onshore Ekman transport of cold fresh Antarctic Surface Water, yielding a 'fresh shelf' regime (Fig. 4a). This wind-driven flow piles up cold fresh water over the continental shelf, inducing a down-welling circulation and, via geostrophic adjustment, a strong Antarctic Slope Current[110]. In these locations, weak cross-slope exchange across the Antarctic Slope Current yields a strong front separating cold fresh waters from warm salty CDW offshore (Fig. 4c), limiting CDW intrusion. Elsewhere, a 'dense shelf' regime prevails in the Ross Sea, Adélie Coast, and around Prydz Bay (Fig. 4d). Here, the overflow of dense shelf water (also referred to as High Salinity Shelf Water in some sectors) is balanced in part by onshore CDW transport, although strong water-mass transformation over the shelf cools these regions during winter[111]. Poleward Ekman transport of cold fresh surface water still occurs, but the Antarctic Slope Current is weaker and less of a barrier to cross-shelf exchange. Finally, along the coast of Wilkes Land a limited 'warm shelf' regime exists (Fig. 4e), where weaker easterly winds enable modified CDW intrusions closer to the ice margin. Recent evidence of a localised warm shelf regime close to Shirase Glacier (Fig. 1d), Dronning Maud Land, has also been detected[112], again enabled by weaker polar easterlies.

Observations of shelf-water temperature trends are extremely sparse around East Antarctica, with few multi-decadal measurements available (e.g. in the Ross Sea)[113,114]. Evidence for long-term shelf-water warming is therefore limited, but warm waters have been detected close to several major outlet glaciers[26-29,112,115], coinciding with high basal melt rates

beneath ice shelves (Fig. 4b)[12-15,116]. This can lead to ice shelf thinning and reduced buttressing, increasing ice discharge[18]. Warm water entering ice shelf cavities can also form basal channels, causing localised incision and further structural weakening[117], including transverse fractures associated with calving[118].

One region where ocean forcing is impacting ice dynamics is Wilkes Land, overlying the ASB and referred to as East Antarctica's 'weak underbelly'[30,119]. A signal of mass loss has emerged over the last three decades[3-9,23], with one study[9] suggesting mass loss (-51 ±80 Gt yr^{-1}: 2016–2020) may be ten times higher than a decade ago. Observations[26-28] have confirmed modified CDW proximal to Moscow University and Totten glaciers (Fig. 4b). Totten's catchment has been thinning and losing mass since the late-1970s, with numerous studies attributing this to ocean forcing and wind-driven upwelling of modified CDW[4-6,11,24,27,32-34,50,120-123]. Its grounding line has been retreating since at least the 1990s[17,33-34] (Fig. 3a) and, given Totten's large catchment (3.9 m of SLE)[33] and high discharge (~70 Gt yr^{-1})[4], these observations are concerning. However, ice discharge may have slowed recently (2008–2017)[4,123], and some variability in basal melting may reflect intrinsic oceanic processes[50]. Furthermore, the grounding line of both Totten and Moscow University glaciers sit on prograde slopes extending 50-60 km up-ice[10], suggesting that imminent Marine Ice Sheet Instability is unlikely.

Elsewhere in Wilkes Land, glaciers entering Porpoise Bay have received much less attention, but have experienced pronounced thinning[5-7] and are sensitive to buttressing from landfast sea-ice[37]. Frost Glacier has the largest catchment (0.84 m SLE)[4] and underwent moderate thinning (<0.5 m yr^{-1}) over recent decades[5,7,11], concomitant with grounding line retreat[17] (>200 m yr^{-1} from 2010–2016) (Fig. 3b). Holmes Glacier is smaller (0.12 m SLE)[4], but the surface thinning (>1 m yr^{-1}) is greater[7,11], perhaps driven by enhanced ice shelf basal melting[12,116] (Fig. 4b). Both glaciers merit monitoring given their large catchments, high discharge, and sensitivity to ocean processes[37]. Likewise, glaciers draining the ASB into Vincennes Bay are largely unstudied, but lie proximal to some of East Antarctica's warmest intrusions of modified CDW[29]. Bond and Underwood glaciers have increased in flow speed (2008–2016)[3,4]; and the grounding line of Vanderford (Fig. 4b) retreated >800 m yr^{-1} from 1996–2017[4], the highest reported rate for East Antarctica (Fig. 3a).

Further west, Denman Glacier (Fig. 4b) holds ~1.5 m SLE[4] in the ASB. Its grounding line sits atop a deep canyon extending >3,500 m below sea level[10,35]. Both its grounded (17 ±4%) and floating (36 ±5 %) portions accelerated[124] from 1972–2017, accompanied by surface thinning since at least the 1990s[5,24,32]. Denman lost a lateral pinning point during its last major calving event (1984)[124] and, from 1996–2017, the western part of its grounding line retreated 5.4 km along a deep trough[10,17,35]. Ice shelf melt rates of >45 ±4 m yr^{-1} (2011–2014)

occur near the grounding line[35] (Fig. 4b), comparable to the highest rates in West Antarctica[12]. One study[4] estimated mass loss from Denman's catchment equivalent to 0.5 mm of sea-level rise from 1979–2017, second only to Totten (0.7 mm) in East Antarctica, but the drivers of any imbalance are unclear given large uncertainties in mass input and limited changes in ice discharge[3,4].

Whilst palaeo-records indicate that the neighbouring WSB retreated during past warm periods, current observations provide limited evidence of change. Cook Glacier has attracted attention due to its large size (~1.6 m SLE)[4] and proximity to a retrograde bed-slope[31]. Its western outlet lost its ice shelf between 1973 and 1989 and subsequently doubled in speed; while the eastern outlet has accelerated since the 1970s[38]. Observations reveal ice surface thinning since at least the 1990s[5,11,120-122], and a small dynamic imbalance (0.2 mm to SLR: 1979–2017)[4], albeit with large uncertainties. Periodic calving events have occurred at the neighbouring Ninnis Glacier[125] (Fig. 2b), also deemed vulnerable to Marine Ice Sheet Instability[10,4], and at Mertz[126]; but without any dynamic response due to negligible buttressing. Limited evidence of current change in glaciers draining the WSB is consistent with low basal melt rates[12-14,116] and a dense shelf regime (Fig. 4a), but ice shelf retreat/calving[30,36,38] in the 1940s to 1980s is suggestive of warmer than present conditions. Hence, recent ocean forcing in this region (difficult to measure due to high volumes of sea-ice/mélange), may not capture the full range of inter-decadal variability.

East Antarctica's other major marine basin – the RSB – is drained by several large glaciers with retrograde slopes (e.g. Recovery, Bailey, Slessor)[127] and may be highly vulnerable to future ocean warming[45], but there is currently no evidence of changes in ice dynamics[3,4,17]. Elsewhere, few glaciers have been studied in East Antarctica's terrestrial sectors, with no obvious changes reported. In Victoria and Oates Land, for example, numerous glaciers have large, unconfined ice tongues that calve periodically, but with no trends in frontal position or ice velocity since the 1970s[30,36,125,128]. The large region encompassing Mac. Robertson Land to Dronning Maud Land is characterised by ice sheet thickening[5,6,11,24,32] due to increased accumulation[47,48] (Fig. 4a), with some evidence of grounding line advance[17] and most catchments gaining mass[3,4]. Shirase – the fastest-flowing glacier in East Antarctica (~2,500 m yr^{-1}) – experiences relatively high basal melt rates (7–16 m yr^{-1})[112] and may have thinned in the 1990s[5,24], but is currently in balance[129] or gaining mass[4].

In summary, the vast majority of East Antarctic outlet glaciers show no discernible change in velocity or discharge over recent decades[3,4], including those draining two of the three marine basins (WSB, RSB). However, some glaciers draining the ASB in Wilkes Land appear to be losing mass in response to ocean heat forcing, similar to glaciers in the WAIS, and with potential for this to be sustained or even increase.

5. Recent Surface Mass Balance

The large spread in estimates of EAIS mass balance (Fig. 2) is derived largely from uncertainties in mass input (surface mass balance: SMB), rather than ice discharge. The mean annual EAIS SMB (1980-2018) over grounded ice has been estimated at +1,247 Gt yr^{-1} from MERRA-2 global reanalysis data[7] and +1,290 Gt yr^{-1} from the MAR regional atmospheric climate model[130] (Fig. 5a). The SMB is dominated by snowfall, with other components (rainfall, sublimation, blowing snow erosion/deposition, runoff) at least an order of magnitude smaller[131].

While most of East Antarctica is relatively dry with typical (interquartile) annual snowfall ranging from 0.05–0.14 meters water equivalent[131], the area is vast. Thus, atmospheric variability (and snowfall) on time-scales from hours to decades[51] is imprinted on overall mass balance. Indeed, inter-annual variations in SMB (e.g. 1980–2018: σ = 106 and 91 Gt yr^{-1} for MERRA-2 and MAR, respectively; Fig. 5a) are comparable to the signal of overall mass change (Fig. 2), highlighting the sensitivity of SMB to short-lived but extreme events and the need for long observational time-series (>10s of years).

The absence of an EAIS-wide array of direct snow accumulation observations means that assessments of SMB rely on atmospheric datasets, atmospheric reanalyses and regional climate models. However, the lack of observations available for assimilation into global reanalyses, and the regional climate models forced by those reanalyses, means that the representation of atmospheric circulation over the EAIS is poorly constrained. This contributes to the large spread in SMB estimates, exacerbating uncertainty in overall mass change. A recent comparison of Antarctic SMB in eight regional climate models[132] found the range in basin-wide SMB varied from ~3% to ~40% of the model mean. Model differences were greatest in the large, dry basins of Adélie and Victoria Land, whilst high accumulation basins (e.g. Wilkes Land) showed more consensus.

Although the mean SMB of models varies substantially, they broadly agree on the magnitude of inter-annual variability, as well as on recent trends[131,133]. Both MERRA-2[7] and MAR[130] show no significant change in EAIS SMB over the last 40 years (<0.1% per year from 1980–2018: Fig. 5a). Shallow ice/firn core analyses[133,134] indicate this forms part of a century of no significant change (1901–2000 SMB trend = 0.1 ± 0.4 Gt yr^{-2}). Over the period 1800–2000, however, a trend of increased accumulation has been reported[133] (0.3 ± 0.1 Gt yr^{-2}), but substantial low-frequency variability increases the uncertainty, suggesting it may be insignificant[51]. Furthermore, due to their relatively short (<20 years) observational record, altimetry and gravimetry methods do not fully capture these decadal-to-century variations in

SMB, which can complicate the separation of SMB and ice dynamical change. Long-term SMB variations, while relatively unconstrained, are also essential to correct altimetry records for changes in firn air content.

Recently, ponding of meltwater on East Antarctic ice shelves has received considerable attention[135-139] due to its potential role in ice shelf collapse via hydro-fracturing[44,85,140-142]. Surface meltwater (streams, lakes, slush), found in the grounding zone of numerous East Antarctic ice shelves[136], indicates insufficient porosity for drainage into the firn. Where firn air content is high, meltwater drains into the firn and may refreeze[142]. Firn air content can be approximated by a liquid-to-solid ratio, defined by the amount of surface melt (and rainfall, rare over East Antarctica[143]) divided by snowfall. Although subject to uncertainties (particularly the liquid component in the marginal areas of the ice sheet), liquid-to-solid ratios are relatively easy to compute and are <25% on most East Antarctic ice shelves (Fig. 5c), indicating annual snowfall is >4 times larger than liquid water fluxes and that a porous firn layer (10s m) accommodates storage/refreezing of summer meltwater. Notable exceptions include the grounding zones of Amery Ice Shelf, with liquid-to-solid ratios up to 80% (similar to Antarctic Peninsula ice shelves), and some eastern Dronning Maud Land ice shelves (~40%). These ice shelves support high densities of supraglacial lakes[136,137,139], but their physical confinement and thickness (e.g. Amery) protect them from widespread hydrofracture. Indeed, ice shelf collapse via hydrofracturing is critically dependent on stress conditions, with <1% of vulnerable ice shelf areas in East Antarctica currently supporting lakes[141].

Given that surface melt has not significantly increased in any of East Antarctica's drainage basins over the last 40 years (Fig. 5b) and that snowfall has remained broadly the same, and increased over western East Antarctica, we suggest few ice shelves are currently at risk from hydrofracture. However, climate projections indicate surface melt and rainfall (especially on East Antarctic ice shelves), as well as snowfall (over the entire EAIS), will increase in the next century[143-149]. This will increase the vulnerability of the northernmost ice shelves[130,142,147,149], such as West and Shackleton[130,140,141]. Shackleton, partially fed by Denman Glacier, already hosts high densities of supraglacial lakes[136,138], experiences high basal melt rates (Fig. 4b), and is considered most at risk[141,149].

6. Future Projections

Since the 2013 IPCC report[150], there has been significant progress in understanding the uncertainties associated with modelling future ice sheet response in Antarctica. Here, we focus on projections that partition the EAIS-only sea-level contribution at 2100, 2300 and 2500 (Fig. 6).

Using the IPCC (2013)[150] method gives median EAIS sea-level contributions of +0.5 to +0.8 cm at 2100 (Fig. 6a: 'IPCC 2013 updated'). Here, the dynamic response was extrapolated from observations and does not vary with emissions scenario, and the SMB response to warming was derived from climate models (recalculated here for Shared Socioeconomic Pathways (SSPs), using temperature projections from the IPCC (2021)[151]). More recent studies generate a wider range of projections with both negative and positive sea-level contributions from the EAIS by 2100, some of which approach +15 cm or more under very high emissions[43,152,153] (Fig. 6a). The Ice Sheet Model Intercomparison Project (ISMIP6) for the sixth phase of the Coupled Model Intercomparison Project (CMIP6) represents the most comprehensive and up-to-date synthesis of these projections[25,148,152,154], using eleven ice sheet models forced by six CMIP5[149] and four CMIP6[25] climate models. Experiments include high and low emission scenarios (RCP8.5/SSP5-85 and RCP2.6/SSP1-26, respectively), a range of parameter values governing the sensitivity of ice shelf basal melting to ocean temperatures[155], and various scenarios of ice shelf collapse driven by atmospheric forcing[144]. Overall, ISMIP6 gives an EAIS-only sea-level contribution ranging from -7 to +15 cm at 2100 (Fig. 6a).

A major uncertainty is the balance between the SMB input (influenced by the choice of climate model) and dynamic losses (largely influenced by the choice of basal melt sensitivity to ocean warming). A comparison of ISMIP6 simulations driven by two different global climate models under RCP8.5, for example, can change the sign of overall mass balance (Fig. 6a: 'ISMIP6: GCM1' versus 'GCM 2'). A similar effect is seen when comparing ISMIP6 simulations using two distributions of the parameter governing basal melting: one derived from the Antarctic average, and the other from a high-melt region proximal to Pine Island Glacier, WAIS (Fig. 6a: 'ISMIP6: mean melt' versus 'high melt').

The ISMIP6 ensemble was unavoidably relatively small (344 simulations from 14 modelling groups) and unevenly sampled. Recently, statistical emulation was used[152] to resample the uncertainties, giving median projections from the EAIS at 2100 (+1.5 to +2.6 cm) that are 2-3 cm higher than the original ensemble means (Fig. 6a: 'ISMIP: all' versus 'ISMIP6 emulator'). This is partly due to the greater weight given to high basal melt values[152], and partly due to the updated IPCC (2021) projections, which have a mean increase of +1.1 cm arising mostly from the estimated response to pre-2015 climate change[151]. The influence of the basal melt sensitivity can also be seen in the dynamic-only contributions from the Linear Antarctic Response to basal melting Model Intercomparison Project phase 2 (LARMIP-2)[156], recalculated here with IPCC (2021)[151] temperature projections (Fig. 6b). The ISMIP6 emulator projects similar 5th to 95th percentiles to LARMIP-2, but much higher medians (+9 to +10 cm), under a 'risk-averse' scenario[152] (Fig. 6b): a subset of climate and ice sheet models that lead

399 to high mass loss via high basal melting and ice shelf disintegration. The SMB contribution to
400 sea level is not modelled by LARMIP-2 but is expected to be negative, lowering the total sea-
401 level contribution (LARMIP-2's EAIS region is also smaller than other studies). After adding
402 the estimated SMB input (median -2 to -5 cm SLE), the IPCC (2021)[151] found that differences
403 between LARMIP-2[156] and the ISMIP6 emulator[152] could largely be explained by different
404 assumptions about basal melt sensitivity, and combined the two for the main assessment with
405 a 'p-box' approach (mean of the two individual medians gives the assessed median; outer
406 edges of the individual 17-83rd percentiles gives the outer edges of the assessed *likely* (17-
407 83%) ranges). Taking the same 'p-box' approach with LARMIP-2 and ISMIP6 here gives the
408 combined median EAIS contributions of +1 to +3 cm by 2100 across all scenarios, with 5th
409 percentiles of -3 to -5 cm, and 95th percentiles of +15 to +17 cm (SSP1-2.6), +16 to +19 cm
410 (SSP2-4.5), and +20 to +25 cm (SSP5-8.5).

411 Even higher projections at 2100 have been made by incorporating the proposed
412 'Marine Ice Cliff Instability' [44,85], which involves the collapse of deep ice cliffs at the grounding
413 line, initiated by ice shelf disintegration (Fig. 6b: lower section). This mechanism has been
414 added to one ice sheet model[44,85], motivated by theoretical considerations and observations
415 of ice cliff calving mechanics, and for this model to be able to simulate the highest potential
416 Pliocene sea level contributions (Fig. 1b). The inclusion and representation of an ice-cliff
417 instability are debated[68,86,151,157-159] and the timing of ice shelf disintegration is highly
418 uncertain[151]. Indeed, projections using marine ice-cliff instability[46] are extremely sensitive to
419 warming, with negative contributions under low and medium emissions, but a 95th percentile
420 of +38 cm under very high emissions (Fig. 6b). Expert elicitation[160] does not explicitly define
421 contributing processes, but encompasses the full range of model projections under very high
422 emissions and is narrower for low emissions (Fig. 6b). Both marine ice-cliff instability and
423 expert elicitation were assessed by the IPCC (2021)[151] as *low confidence* projections - that
424 could nevertheless not be ruled out - and were combined with the main projections in a p-box
425 approach. Taking a similar approach here gives a *low confidence* 95th percentile of +47 cm
426 SLE from the EAIS at 2100 under SSP5-8.5.

427 Few scenario-dependent EAIS projections are available beyond 2100. Maximum
428 contributions under low and medium emissions are +0.6 m SLE at 2300 (Fig. 6c) and +0.7 m
429 at 2500 (Fig. 6d). This suggests the EAIS contribution to sea-level would be well under +1 m
430 over the next few centuries if emissions follow current Nationally Determined Contributions,
431 which are lower than the medium scenario (SSP2-4.5)[161]; and less than +0.5 m under low
432 emissions with a median warming of <2°C (SSP1-2.6 95th percentile at 2300 is 2.2°C)[151].

433 Under very high emissions, model projections show a wide range, with the EAIS
434 contributing -0.08 to +3.0 m SLE at 2300 (Fig. 6c, upper panel) and +1.0 to +5.4 m at 2500

435 (Fig. 6d), although the upper bounds would halve (1.3 m at 2300 and 2.3 m at 2500) when
436 excluding the study[44] that the IPCC (2019)[68] deemed to over-estimate ice shelf collapse. *Low*
437 *confidence* projections using marine ice-cliff instability[46] and from expert elicitation[160] are even
438 higher (Fig. 6c, lower), with 95th percentiles of +4.7 m and +3.9 m at 2300, respectively,
439 although most of the elicited distribution is far lower (83rd percentile 0.2 m SLE). Taking the
440 IPCC (2021)[151] p-box approach to combine these gives a *low confidence* 95th percentile
441 approaching +5 m at 2300. Such high emissions are becoming increasingly less probable, as
442 they would greatly exceed those predicted for Nationally Determined Contributions under the
443 Paris Agreement and other pledges (e.g. net zero emissions by mid-late century)[161].

444 Spatial patterns of modelled mass loss consistently highlight the vulnerability of East
445 Antarctica's marine-based sectors, but the magnitude and rate of ice loss is model-dependent.
446 Multi-century simulations[43,44,46,148,162,163] typically show grounding line retreat and mass loss in
447 the ASB (Fig. 1f), followed by the WSB and RSB, although the latter shows high sensitivity to
448 ocean warming in some studies[45,163]. Notably, most models do not include recent discoveries[10]
449 of over-deepened subglacial topography that might exacerbate Marine Ice Sheet Instability,
450 such as the deep trough connecting Denman Glacier to the ASB. Given that large parts of
451 East Antarctica remain unsurveyed[10], there may be undiscovered over-deepenings upstream
452 of grounding lines or unknown bathymetric troughs with potential to carry warm waters towards
453 the ice margin: both could increase mass loss beyond current expectations.

454 Future ocean conditions will exert a critical influence on ice discharge via basal melting
455 and ice shelf buttressing[12-18]. However, coupled global ocean-climate models do not resolve
456 important processes, such as circulation within sub-ice-shelf cavities, tidal flows and eddies,
457 and gradients across the Antarctic Slope Current. This leaves global models with baseline
458 biases in hydrographic properties over the continental shelf and shelf-break, although multi-
459 model means are more realistic[164]. Insights can be gained from examining climate projections
460 in terms of future surface atmospheric warming, sea-ice melt, wind and ocean circulation
461 changes, and shelf-water hydrography. Projected atmospheric circulation changes include an
462 on-going poleward shift and strengthening of the Southern Hemisphere westerly jet across all
463 seasons[165], and a weakening of the coastal easterlies during austral summer and autumn,
464 particularly around East Antarctica[146]. These wind changes are likely to weaken the Antarctic
465 Slope Current, enabling enhanced CDW intrusions onto the shelf[166,167], particularly around
466 Wilkes Land and west to Prydz Bay. Projected surface warming and the addition of meltwater
467 also enhances vertical stratification over the shelf, reducing or shutting down dense shelf water
468 formation[168] and leaving the deep-shelf waters warmer. Meltwater input from ice shelves may
469 also create a positive feedback, with additional freshening driving sub-ice-shelf warming,
470 leading to further melt[169,170], as hypothesised for the last deglaciation[108]. Sea-ice loss also

reduces albedo over the ocean, driving further warming[171] and increasing the vulnerability of outlet glaciers to ice shelf/tongue collapse[37]. However, climate models have typically struggled to reproduce Antarctic sea-ice trends[172], which are improved when ice shelf melt[173] and improved representations of sea-ice motion[174] are included.

7. Lessons from the Past Inform the Future

Evidence from the palaeo-record and numerical modelling highlight the sensitivity of East Antarctica's major marine basins (the ASB, WSB and RSB) to past warm periods, including significant ice loss during the early to Mid-Miocene (24–14 Ma), and a multi-metre sea-level contribution during the mid-Pliocene (5.3–2.6 Ma), when atmospheric CO_2 concentrations were comparable to present-day. Retreat of the WSB during more recent interglacials (marine isotope stage 11) further highlights its sensitivity to modest warming scenarios (1.5–2°C). During the last deglaciation, however, there were only limited changes to the ASB and WSB, with grounding line retreat focussed in the marine embayments of the Ross and Weddell Seas that connect the WAIS and EAIS (Fig. 1c). Here, retreat has been linked to a positive feedback driven by ocean warming, whereby meltwater input freshened surface waters, facilitating increased incursions of modified CDW onto the continental shelf, continuing into the Holocene[108]. This mechanism, coupled with evidence of Marine Ice Sheet Instability across major over-deepenings during deglaciation, illustrates a plausible scenario for destabilising some major East Antarctic outlet glaciers over the next few centuries (e.g. Denman). Furthermore, there are signs that some glaciers draining the ASB in Wilkes Land are currently losing mass, with grounding line retreat and ice surface thinning rates comparable to, and sometimes exceeding, millennial-scale rates of change during the last deglaciation (Fig. 3); and raising the possibility that a longer-term dynamic response to ocean forcing is underway. However, the WSB and RSB currently show limited evidence of change; even though the latter is deemed most vulnerable to future ocean warming[45] and may already be exposed to periodic intrusions of modified CDW[175] that could increase later this century[176].

Current understanding is therefore insufficient to determine if and when specific thresholds of instability might be reached in East Antarctica's three marine-based sectors. Indeed, there is no single EAIS response, or time-scale of response, and estimates of overall mass balance may obscure emerging trends of mass loss from some catchments. Furthermore, recent and future trends in SMB, dominated by snowfall, are subject to extreme inter-annual variability and large uncertainties. These uncertainties, together with limited data to inform models of glacio-isostatic adjustment and corrections for firn air content, lead to satellite-based estimates of EAIS mass balance with large uncertainties.

Future work should continue to target early-warning signs of dynamic imbalance in the three major marine basins, such as ice surface thinning propagating upstream from retreating grounding lines, together with ice flow acceleration and ice shelf thinning. There remains an urgent need to understand the sensitivity of basal melting to ocean temperatures, and for more detailed observations of continental shelf bathymetry, bedrock topography proximal to, and up-ice from, current grounding lines, and improved observations of sub-shelf cavities and oceanic processes. These observations should be supplemented with more widespread and systematic palaeo-campaigns on East Antarctic continental shelves to constrain the sensitivity of catchments to past ocean-climate forcing (e.g. the RSB), including rates of change and potential tipping points. Such data can inform numerical modelling, where multi-model and perturbed parameter ensembles are required to improve the robustness of multi-century projections.

Despite current uncertainties, surface melt and rainfall (particularly on ice shelves), and snowfall (over the entire EAIS), will increase this century. By combining the 'ISMIP6 emulator' with 'LARMIP-2 updated' (Fig. 6b) and an intermediate IPCC (2021) SMB estimate, we find the EAIS makes a small positive contribution to sea level (+2 cm) at 2100, but with a wide range depending on scenario (5^{th} to 95^{th} percentiles: -4 cm to +16-22 cm), and with upper bounds driven by high basal melt sensitivity to warming. *Low confidence* projections, due to limited evidence, reach +0.47 m at 2100 under very high emissions (Fig. 6b). If warming continues beyond 2100, sustained by high emissions, evidence from the palaeo-record, recent observations, and numerical modelling projections (albeit derived from a small number of studies) point to significant potential contributions to global mean sea level from marine-based sectors, reaching ~1-3 m or more by 2300 (Fig. 6c) and ~2-5 m by 2500 (Fig. 6d). Catchments most at risk drain the ASB in Wilkes Land (Frost, Holmes, Totten, Vanderford, Denman, Moscow University), and the WSB in George V Land (Cook, Ninnis), with the RSB also potentially vulnerable. Crucially, if the Paris Agreement to limit warming to well below 2°C above pre-industrial is satisfied, significant mass loss could be reduced or averted (Fig. 6c, d: SSP1-2.6/RCP2.6), with the EAIS sea-level contribution remaining below +0.5 m at 2500. Even under emissions similar to Nationally Determined Contributions which exceed this temperature target (Fig 6c, d: SSP2-4.5/RCP4.5), East Antarctica's contribution to sea-level rise would remain well below +1 m over the coming centuries. The fate of the world's largest ice sheet remains very much in our hands.

Author Contributions:

CRS developed the idea for the paper and all authors provided input on its initial contents and structure. CRS drafted Section 1. GJGP and SSRJ drafted Section 2, with contributions from MJB and TvdF. RSJ drafted Section 3 with contributions from MJB. CRS and BWJM drafted Section 4, with contributions from MHE and AF. JTML and BM drafted Section 5 with input from MAK. CR and TLE drafted Section 6, with contributions from MHE. CRS drafted Section 7 with input from TLE. All authors provided comments and edits on all sections of the paper. GJGP produced Fig. 1, with input from CRS. PLW produced Fig. 2 with input from CRS, MAK and RSJ. RSJ produced Fig. 3, with input from BWJM and CRS. AF, MHE and BWJM produced Fig. 4. JTML and BM produced Fig. 5. TLE carried out the analysis and produced Fig. 6 with input from CR.

Competing Interests:

The authors declare no competing interests.

References:

1. The IMBIE team. Mass balance of the Antarctic Ice Sheet from 1992 to 2017. *Nature* **558**, 219-222 (2018).
2. Bamber, J.L., Westaway, R.M., Marzeion, B. & Wouters, B. The land ice contribution to sea level during the satellite era. *Environ. Res. Lett.* **13**, 063008 (2018).
3. Gardner, A.S. et al. Increased West Antarctic and unchanged East Antarctic ice discharge over the last 7 years 2018. *Cryosphere* **12**, 521–547 (2018). **Uses ice surface velocity datasets and a surface mass balance model to suggest that, overall, ice discharge from glaciers draining the East Antarctic Ice Sheet was remarkably stable between ~2008 and 2013/15, whereas those in West Antarctica increased.**
4. Rignot, E. et al. Four decades of Antarctic Ice Sheet mass balance from 1979-2017. *Proc. Natl. Acad. Sci. U.S.A.* **116** (4), 1095–1103 (2019). **Uses updated drainage inventory, ice thickness and ice velocity data, together with a surface mass balance model, to calculate Antarctic Ice Sheet mass balance (1979-2017) and suggest that East Antarctica was a major participant in mass loss.**
5. Schröder, L. et al. Four decades of surface elevation change of the Antarctic Ice Sheet from multi-mission satellite altimetry. *Cryosphere* **13**, 427-449 (2019).
6. Shepherd, A. et al. Trends in Antarctic ice sheet elevation and mass. *Geophys. Res. Lett* **46**, 8174-8183 (2019).
7. Smith, B. et al. Pervasive ice sheet mass loss reflects competing ocean and atmosphere processes. *Science* **368**, 1239–1242 (2020).
8. Velicogna, I. et al. Continuity of ice sheet mass loss in Greenland and Antarctica from the GRACE and GRACE Follow-On missions. *Geophys. Res. Lett*. **47**, e2020GL087291 (2020).
9. Wang, L., Davis, J.L. & Howat, I.M. Complex patterns of Antarctic ice sheet mass change resolved by time-dependent rate modelling of GRACE and GRACE follow-on observations. *Geophys. Res. Lett.* **48** (1), e2020GL090961 (2021). **Introduces a novel approach for analysing satellite gravimetry observations to estimate time-varying mass-change rates in Antarctica and finds a continuously accelerating trend of mass loss in Wilkes Land, East Antarctica, over the last two decades**
10. Morlighem, M. et al. Deep glacial troughs and stabilizing ridges unveiled beneath the margins of the Antarctic ice sheet. *Nat. Geosci*. **13**, 132-137 (2020).
11. Pritchard, H. D., Arthern, R. J., Vaughan, D. G., & Edwards, L. A. Extensive dynamic thinning on the margins of the Greenland and Antarctic ice sheets. *Nature* **461**, 971–975 (2009).
12. Pritchard, H.D. et al. Antarctic ice-sheet loss driven by basal melting of ice shelves. *Nature* **484**, 502-505 (2012).
13. Depoorter, M.A. et al. Calving fluxes and basal melt rates of Antarctic ice shelves. *Nature* **502** (7469), 89-92 (2013).
14. Rignot, E., Jacobs, S., Mouginot, J. & Scheuchl, B. Ice-shelf melting around Antarctica. *Science* **341** (6143), 266-270 (2013).

15. Paolo, F.S., Fricker, H.A. & Padman, L. Volume loss from Antarctic ice shelves is accelerating. *Science* **348**, 327-331 (2015).
16. Fürst, J.J. et al. The safety band of Antarctic ice shelves. *Nat. Clim. Change* **6**, 479-482 (2016).
17. Konrad, H. et al. Net retreat of Antarctic glacier grounding lines. *Nat. Geosci.* **11**, 258-262 (2018).
18. Gudmundsson, G.H., Paolo, F.S., Adusumilli, S. & Fricker, H.A. Instantaneous Antarctic ice sheet mass loss driven by thinning ice shelves. *Geophys. Res. Lett*. **46**, 13,903-13,909 (2019).
19. Schoof, C. Ice sheet grounding line dynamics: steady states, stability, and hysteresis. *J. Geophys. Res. Earth Surf.* **112** (F3), F03S28 (2007).
20. Mercer, J.H. West Antarctic ice sheet and CO_2 greenhouse effect: a threat of disaster. *Nature* **271**, 321-325 (1978).
21. Noble, T.L. et al. The sensitivity of the Antarctic Ice Sheet to a changing climate: past, present and future. *Rev. Geophys.* **58**, e2019RG000663 (2020).
22. Sugden, D. E. et al. Preservation of Miocene glacier ice in East Antarctica. *Nature* **376**, 412-414 (1995).
23. Davis, C.H., Li, Y., McConnell, J.R., Frey, M.M. & Hanna, E. Snowfall-driven growth in East Antarctic Ice Sheet mitigates recent sea-level rise. *Science* **308** (5730), 1898-1901 (2005). **One of the earlier studies to use satellite radar altimetry to show that sea-level rise was mitigated by snowfall-driven growth of the East Antarctic Ice Sheet (1992-2003).**
24. Zwally, H.J. et al. Mass changes of the Greenland and Antarctic ice sheets and ice shelves and contributions to sea level rise: 1992-2002. *J. Glaciol.* **51** (175), 509-527 (2005).
25. Payne, A.J. et al. Future sea level change under the Coupled Model Intercomparison Project Phase 5 and Phase 6 scenarios from the Greenland and Antarctic ice sheets. *Geophys. Res. Lett*. **48**, e2020GL091741 (2021).
26. Greenbaum, J.S. et al. Ocean access to a cavity beneath Totten Glacier in East Antarctica. *Nat. Geosci.* **8** (4), 294-298 (2015).
27. Rintoul, S.R. et al. Ocean heat drives rapid basal melt of the Totten Ice Shelf. *Sci. Adv.*, **2**, e1601610 (2016). **Presents observations from the calving front of Totten Glacier, East Antarctica, that confirm warm water enters the ice shelf cavity through a deep channel, driving high basal melt rates.**
28. Silvano, A., Rintoul, S.R., Pena-Molino, B. & Williams, G.D. Distribution of water masses and meltwater on the continental shelf near the Totten and Moscow University ice shelves. *J. Geophys. Res. Oceans* **122** (3), 2050-2068 (2017).
29. Ribeiro, N. et al. Warm modified Circumpolar Deep Water intrusions drive ice shelf melt and inhibit Dense Shelf Water formation in Vincennes Bay, East Antarctica. *J. Geophys. Res. Oceans* **126**, e20202JC016998 (2021).
30. Miles, B.W.J., Stokes, C.R. & Jamieson, S.S.R. Pan-ice-sheet glacier terminus change in East Antarctica reveals sensitivity of Wilkes Land to sea-ice changes. *Sci. Adv.* **2** (5), 1-7 (2016).
31. Mengel, M. & Levermann, A. Ice plug prevents irreversible discharge from East Antarctica. *Nat. Clim. Change* **4**, 451–455 (2014).
32. Flament, T. & Rémy, F. Dynamic thinning of Antarctic glaciers from along-track repeat radar altimetry. *J. Glaciol.* **58** (211), 830-840 (2012).
33. Li, X., Rignot, E., Morlighem, M., Mouginot, J. & Scheuchl, B. Grounding line retreat of Totten Glacier, East Antarctica, 1996 to 2013. *Geophys. Res. Lett*. **42**, 8049–8056 (2015).
34. Li, X., Rignot, E., Mouginot, J. & Scheuchl, B. Ice flow dynamics and mass loss of Totten Glacier, East Antarctica, from 1989 to 2015. *Geophys. Res. Lett*. **43**, 6366–6373 (2016).
35. Brancato, V. et al. Grounding line retreat of Denman Glacier, East Antarctica, measured with COSMO-SkyMed radar interferometry Data. *Geophys. Res. Lett*. **47**, e2019GL086291 (2020). **Presents observations of rapid grounding line retreat (1996-2017/18) along a deep trough from an East Antarctic glacier holding 1.5 m sea level rise equivalent.**
36. Miles, B.W.J., Stokes, C.R., Vieli, A. & Cox, N.J.C. Rapid, climate-driven changes in outlet glaciers on the Pacific coast of East Antarctica. *Nature* **500** (7464), 563-566 (2013).
37. Miles, B.W.J., Stokes, C.R. & Jamieson, S.S.R. Simultaneous disintegration of outlet glaciers in Porpoise Bay (Wilkes Land), East Antarctica, driven by sea-ice break-up. *Cryosphere*, **11** (1), 427-442 (2017).
38. Miles, B.W.J., Stokes, C.R. & Jamieson, S.S.R. Velocity increases at Cook Glacier, East Antarctica, linked to ice shelf loss and a subglacial flood event. *Cryosphere* **12** (10), 3123-3136 (2018).
39. Cook, C.P. et al. Dynamic behaviour of the East Antarctic ice sheet during Pliocene warmth. *Nature Geosci.* **6**, 765-769 (2013). **Suggests that changes in the provenance of sedimentary material on the Wilkes Land continental shelf can be linked to shifts in the position of the East Antarctic Ice Sheet margin and resulting erosional pathways.**
40. Cook, C.P. et al. Sea surface temperature control on the distribution of far-travelled Southern Ocean ice-rafted detritus during the Pliocene. *Paleoceanography* **29**, 533-538 (2014).

41. Wilson, D.J. et al. Ice loss from the East Antarctic Ice Sheet during late Pleistocene interglacials. *Nature* **561**, 383-386 (2018).
42. Blackburn, T. et al. Ice retreat in Wilkes Basin of East Antarctica during a warm interglacial. *Nature* **583**, 554-559 (2020).
43. Golledge, N.R. et al. The multi-millennial Antarctic commitment to future sea-level rise. *Nature* **526**, 421-425 (2015).**Uses a coupled ice-sheet/ice-shelf model to show that if atmospheric warming exceeds 1.5 to 2 degrees Celsius above present, collapse of ice shelves triggers a centennial- to millennial-scale response that includes substantial contributions from East Antarctica's marine basins under 'high' scenarios.**
44. DeConto, R.M. & Pollard, D. Contribution of Antarctica to past and future sea-level rise. *Nature* **531**, 591-597 (2016).
45. Golledge, N.R., Levy, R.H., McKay, R.M. & Naish, T.R. East Antarctic ice sheet most vulnerable to Weddell Sea warming. *Geophys. Res. Lett*. **44**, 2343-2351 (2017).
46. DeConto, R.M. et al. The Paris Climate Agreement and future sea-level rise from Antarctica. *Nature* **593**, 83-89 (2021).
47. Boening, C., Lebsock, M., Landerer, F. & Stephens, G. Snowfall-driven mass change on the East Antarctic ice sheet. *Geophys. Res. Lett*. **39**, L21501 (2012). **Reports the addition of 350 Gt of snowfall over the EAIS from 2009 to 2011 from extreme precipitation events, equivalent to a decrease in global mean sea level at a rate of 0.32 mm/yr over this three-year period.**
48. Lenaerts, J.T.M. et al. Recent snowfall anomalies in Dronning Maud Land, East Antarctica, in a historical and future climate perspective. *Geophys. Res. Lett*. **40**, 2684-2688 (2013).
49. Jones, J.M. et al. Assessing recent trends in high-latitude Southern Hemisphere surface climate. *Nat. Clim. Change* **6**, 917-926 (2016).
50. Gwyther, D. E. et al. Intrinsic processes drive variability in basal melting of the Totten Glacier Ice Shelf. *Nat. Commun*. **9**, 3141 (2018).
51. King, M.A. & Watson, C.S. Antarctic surface mass balance: natural variability, noise, and detecting new trends. *Geophys. Res. Lett*. **47**, e2020GL087493 (2020).
52. Zachos, J.C., Breza, J.R. & Wise, S.M. Early Oligocene ice-sheet expansion on Antarctica: Stable isotope and sedimentological evidence from Kerguelen Plateau, southern Indian Ocean. *Geology* **20** (6), 569–573 (1992).
53. Gulick, S.P.S. et al. Initiation and long-term instability of the East Antarctic Ice Sheet. *Nature* **552**, 225-229 (2017).
54. Gasson, E. & Keisling, B.A. The Antarctic Ice Sheet – A paleoclimate modelling perspective. *Oceanography* **33** (2), 90-100 (2020).
55. Naish, T. R. et al. Orbitally induced oscillations in the East Antarctic ice sheet at the Oligocene/Miocene boundary. *Nature* **413**, 719-723 (2001). **Presents evidence of cyclic variability in Ross Sea sediment cores that are linked to the oscillating extent of the East Antarctic Ice Sheet during the Oligocene-Miocene transition.**
56. Levy, R. et al. Antarctic ice sheet sensitivity to atmospheric CO_2 variations in the early to mid-Miocene. *Proc. Natl. Acad. Sci. U.S.A.* **113** (13), 3453-3458 (2016).
57. Gasson, E., DeConto, R.M., Pollard, D. & Levy, R.H. Dynamic Antarctic ice sheet during the early to mid-Miocene. *Proc. Natl. Acad. Sci. U.S.A.* **113** (13), 3459-3464 (2016).
58. Passchier, S. et al. Early and middle Miocene Antarctic glacial history from the sedimentary facies distribution in the AND-2A drill hole, Ross Sea, Antarctica. *Geol. Soc. Am. Bull.* **123**, 2352-2365 (2011).
59. Lewis, A. R. et al. Mid-Miocene cooling and the extinction of tundra in continental Antarctica. *Proc. Natl. Acad. Sci. U.S.A.* **105**, 10676-10680 (2008).
60. Rae, J.W.B. et al. Atmospheric CO_2 over the past 66 million years from marine archives. *Annu. Rev. Earth Planet. Sci.* **49**, 609-641 (2021).
61. Sangiori et al. Southern Ocean warming and Wilkes Land ice sheet retreat during the mid-Miocene. *Nat. Commun.* **9**, 317 (2018).
62. Marshalek, J.W. et al. A large West Antarctic Ice Sheet explains early Neogene sea-level amplitude. *Nature* **600**, 450-455 (2021).
63. Miller, K.G. et al. Cenozoic sea-level and cryospheric evolution from deep-sea geochemical and continental margin records. *Sci. Adv*. **6** (20), eaaz1346 (2020).
64. Lee, J.Y. et al. In, Future global climate: scenario based projections and near-term information. In, *Climate Change 2021: The Physical Science Basis. Contribution of Working Group I to the Sixth Assessment Report of the Intergovernmental Panel on Climate Change* [Masson-Delmotte, V. et al. (eds.)]. Cambridge University Press (in press).
65. Steinthorsdottir, M. et al. The Miocene: the future of the past. *Paleoceanogr. Paleoclimatol*. **36**, e2020PA004037 (2021).

66. Martínez-Botí, M.A. et al. Plio-Pleistocene climate sensitivity evaluated using high-resolution CO_2 records. *Nature* **518**, 49-54 (2015).
67. Haywood, A.M., Dowsett, H.J. & Dolan, A.M. Integrating geological archives and climate models for the mid-Pliocene warm period. *Nat. Commun*. **7**, 1–14 (2016).
68. Oppenheimer, M. et al. Sea level rise and implications for low-lying islands, coasts and communities, Chapter 4. In Pörtner, H.-O. et al. (Eds) *IPCC Special Report on the Ocean and Cryosphere in a Changing Climate* (2019).
69. Dumitru, O.A. et al. Constraints on global mean sea level during Pliocene warmth. *Nature* **574**, 233-236 (2019).
70. Grant, G.R. et al. The amplitude and origin of sea-level variability during the Pliocene epoch. *Nature* **574**, 237-241 (2019).
71. Dutton, A. et al. Sea-level rise due to polar ice-sheet mass loss during past warm periods. *Science* **349** (6244) aaa4019 (2015).
72. Dolan, A.M. et al. Sensitivity of Pliocene ice sheets to orbital forcing. *Palaeogeogr. Palaeoclimatol. Palaeoecol.* **309**, 98-110 (2011).
73. Webb, P.N., Harwood, D.M., McKelvey, B.C., Mercer, J.H. & Stott, L.D. Cenozoic marine sedimentation and ice volume on the East Antarctic craton. *Geology* **12**, 287-291 (1984).
74. Scherer, R., DeConto, R., Pollard, D. & Alley, R.B. Windblown Pliocene diatoms and East Antarctic Ice Sheet retreat. *Nat. Commun.* **7**, 12957 (2016).
75. Bertram, R.A. et al. Pliocene deglacial event timelines and the biogeochemical response offshore Wilkes Subglacial Basin, East Antarctica. *Earth Planet. Sci. Lett.* **494**, 109-116 (2018).
76. Taylor-Silva, B. I. & Riesselman, C.R. Polar frontal migration in the warm late Pliocene: diatom evidence from the Wilkes Land margin, East Antarctica. *Paleoceanogr. Paleoclimatol*. **33**, 76–92. (2018).
77. Williams, T. et al. Evidence for iceberg armadas from East Antarctica in the Southern Ocean during the late Miocene and early Pliocene. *Earth Planet. Sci. Lett.* **290**, 351-361 (2010).
78. Aitken, A.R.A. et al. Repeated large-scale retreat and advance of Totten Glacier indicated by inland bed erosion. *Nature* **533**, 385-389 (2016).
79. Ohneiser, C. et al. Warm fjords and vegetated landscapes in early Pliocene East Antarctica. *Earth Planet. Sci. Lett.* **534**, 116045 (2020).
80. Passchier, S. Linkages between East Antarctic Ice Sheet extent and Southern Ocean temperatures based on a Pliocene high-resolution record of ice-rafted debris off Prydz Bay, East Antarctica, *Paleoceanogr.* **26** (4) PA4204 (2011).
81. Golledge, N.R. et al. Antarctic climate and ice-sheet configuration during the early Pliocene interglacial at 4.23 Ma. *Clim. Past* **13**, 959-975 (2017).
82. De Boer, B. et al. Simulating the Antarctic ice sheet in the late-Pliocene warm period: PLISMIP-ANT, an ice sheet model intercomparison project. *Cryosphere* **9**, 881-903 (2015).
83. Dolan, A.M., de Boer, B., Bernales, J., Hill, D.J. & Haywood, A.M. High climate model dependency of Pliocene Antarctic ice-sheet predictions. *Nat. Commun.* **9**, 2799 (2018).
84. Yan, Q., Zhang, Z. and Wang, H. Investigating uncertainty in the simulation of the Antarctic ice sheet during the mid-Piacenzian. *J. Geophys.Res. Atmos*. **121**, 1559–1574 (2016).
85. Pollard, D., DeConto, R.M. & Alley, R.B. Potential Antarctic Ice Sheet retreat driven by hydrofracturing and ice cliff failure. *Earth Planet. Sci. Lett*. **412**, 112-121 (2015). **Proposes new ice sheet model physics, including parameterisations of marine ice cliff instability, in an attempt to reproduce the marine-based retreat of the East Antarctic Ice Sheet during the mid-Pliocene.**
86. Edwards, T.L. et al. Revisiting Antarctic ice loss due to marine ice-cliff instability. *Nature* **566**, 58-63 (2019).
87. Jones, R. S. et al. Cosmogenic nuclides constrain surface fluctuations of an East Antarctic outlet glacier since the Pliocene. *Earth Planet. Sci. Lett.* **480**, 75-86 (2017).
88. Bradley, S.L., Siddall, M., Milne, G.A., Masson-Delmotte, V. & Wolff, E. Combining ice core records and ice sheet models to explore the evolution of the East Antarctic ice sheet during the Last Interglacial period. *Glob. Planet. Change* **100**, 278-290 (2013).
89. Sutter, J. et al. Limited retreat of the Wilkes Basin ice sheet during the Last Interglacial. *Geophys. Res. Lett*. **47**, e2020GL088131 (2020).
90. Mackintosh, A.N. et al. Retreat history of the East Antarctic Ice Sheet since the Last Glacial Maximum. *Quat. Sci. Rev.* **100**, 10-30 (2014). **Synthesises geological and chronological evidence to constrain the history of the East Antarctic Ice Sheet from ~30,000 years ago to present, highlighting marked regional asynchronicity and that the majority of mass loss occurred between ~12,000 and ~6,000 years ago.**
91. Livingstone, S.J. et al. Antarctic palaeo-ice streams. *Earth Sci. Rev.* **111**, 90-128 (2012).

92. Anderson, J.B. et al. Ross Sea paleo-ice sheet drainage and deglacial history during and since the LGM. *Quat. Sci. Rev.* **100**, 31-54 (2014).
93. Hillenbrand, C.-D. et al. Reconstruction of changes in the Weddell Sea sector of the Antarctic Ice Sheet since the Last Glacial Maximum. *Quat. Sci. Rev.* **100**, 111-136 (2014).
94. Arndt, J.E., Hillenbrand, C.-D., Grobe, H., Kuhn, G. & Wacker, L. Evidence for a dynamic grounding line in outer Filchner trough, Antarctica, until the early Holocene. *Geology* **45** (11), 1035-1038 (2020).
95. Lin, Y. et al. A reconciled solution of Meltwater Pulse 1A sources using sea-level fingerprinting. *Nat. Commun.* 12, 2015 (2021).
96. Weber, M. et al. Millennial-scale variability in Antarctic ice-sheet discharge during the last deglaciation. *Nature* **510**, 134-138 (2014).
97. Hall, B.L. et al. Accumulation and marine forcing of ice dynamics in the western Ross Sea during the last deglaciation. *Nature Geosci.* **8**, 625-628 (2015).
98. King, C. et al. Delayed maximum and recession of an East Antarctic outlet glacier. *Geology* **48** (6), 630-634 (2020).
99. Jones, R.S. et al. Rapid Holocene thinning of an East Antarctic outlet glacier driven by marine ice sheet instability. *Nat. Commun*. **6**, 8910 (2015).
100. White, D.A., Fink, D. & Gore, D.B. Cosmogenic nuclide evidence for enhanced sensitivity of an East Antarctic ice stream to change during the last deglaciation. *Geology* **39**, 23-26 (2011).
101. Spector, P. et al. Rapid early-Holocene deglaciation in the Ross Sea, Antarctica. *Geophys. Res. Lett.* **44**, 7817-7825 (2017).
102. Jones, R. S., Gudmundsson, G. H., Mackintosh, A. N., McCormack, F. S., & Whitmore, R. J. Ocean-driven and topography-controlled nonlinear glacier retreat during the Holocene: southwestern Ross Sea, Antarctica. *Geophys. Res. Lett.* **48**, e2020GL091454 (2021).
103. McKay, R. et al. Antarctic marine ice-sheet retreat in the Ross Sea during the early Holocene. *Geology* **44** (1), 7-10 (2016).
104. Halberstadt, A.R.W., Simkins, L.M., Greenwood, S.L. & Anderson, J.B. Past ice-sheet behaviour: retreat scenarios and changing controls in the Ross Sea, Antarctica. *Cryosphere* **10**, 1003-1020 (2016).
105. Kingslake, J. et al. Extensive retreat and re-advance of the West Antarctic Ice Sheet during the Holocene. *Nature* **558**, 430-434 (2018).
106. Mackintosh, A. et al. Retreat of the East Antarctic ice sheet during the last glacial termination. *Nat. Geosci.* **4**, 195-202 (2011).
107. Whitehouse, P.L., Bentley, M.J. & Le Brocq, A.M. A deglacial model for Antarctica: geological constraints and glaciological modelling as a basis for a new model of Antarctic glacial isostatic adjustment. *Quat. Sci. Rev.* **32** (16), 1-24 (2012).
108. Golledge, N.R. et al. Antarctic contribution to meltwater pulse 1A from reduced Southern Ocean overturning. *Nat. Commun.* **5**, 5107 (2014).
109. Lowry, D.P. et al. Deglacial grounding-line retreat in the Ross Embayment, Antarctica, controlled by ocean and atmosphere forcing. *Sci. Adv.* **5** (8), eaav8754 (2019).
110. Thompson, A.F., Stewart, A.L., Spence, P., & Heywood, K.J. The Antarctic Slope Current in a changing climate. *Rev. Geophys.* **56**, 741–770 (2018).
111. Morrison, A.K., Hogg, A. McC., England, M.H. & Spence, P. Warm Circumpolar Deep Water transport towards Antarctica driven by local dense water export in canyons. *Sci. Adv*. **6** (18), eaav2516 (2020).
112. Hirano, D. *et al.* Strong ice-ocean interaction beneath Shirase Glacier Tongue in East Antarctica. *Nat. Commun*. **11**, 4221 (2020).
113. Jacobs, S. S. & Giulivi, C. F. Large multidecadal salinity trends near the Pacific-Antarctic continental margin. *J. Clim*. **23**, 4508–4524 (2010).
114. Schmidtko, S., Heywood, K. J., Thompson, A. F. & Aoki, S. Multidecadal warming of Antarctic waters. *Science* **346**, 1227-1231 (2014).
115. Herraiz–Borreguero, R. et al. Circulation of modified Circumpolar Deep Water and basal melt beneath the Amery Ice Shelf, East Antarctica, *J. Geophys. Res. Oceans*, **120**, 3098–3112 (2015).
116. Adusumilli, S., Fricker, H.A., Medley, B., Padman, L. & Siegfried, M.R. Interannual variation in meltwater input to the Southern Ocean from Antarctic ice shelves. *Nature Geosci.* **13**, 616-620 (2020).
117. Alley, K.E., Scambos, T.A., Siegfried, M.R. & Fricker, H.A. Impacts of warm water on Antarctic ice shelf stability through basal channel formation. *Nat. Geosci*. **9**, 290-292 (2016).
118. Dow, C.F. et al. Basal channels drive active surface hydrology and transverse ice shelf fracture. *Sci. Adv*. **4**, eaa07212 (2018).
119. Pelle, T., Morlighem, M. & McCormack, F.S. Aurora Basin, the weak underbelly of East Antarctica. *Geophys. Res. Lett*. **47** GL086821 (2020).

120. Rignot, E. Changes in ice dynamics and mass balance of the Antarctic ice sheet. *Phil. Trans. Roy. Soc.* **364** (1844), 1637-1655 (2006).
121. Wingham, D.J., Shepherd, A., Muir, A. & Marshall, G.J. Mass balance of the Antarctic ice sheet. *Phil. Trans. Roy. Soc.* **364**, 1627-1635 (2006).
122. Shepherd, A. & Wingham, D. Recent sea-level contributions of the Antarctic and Greenland Ice Sheets. *Science* **316**, 1529-1532 (2007).
123. Greene, C.A., Blankenship, D.D., Gwyther, E.E., Silvano, A. & van Wijk, E. Wind causes Totten Ice Shelf melt and acceleration. *Sci. Adv.* **3**, e1701681 (2017).
124. Miles, B.W.J. et al. Recent acceleration of Denman Glacier (1972-2017), East Antarctica, driven by grounding line retreat and changes in ice tongue configuration. *Cryosphere* **15**, 663-676 (2021).
125. Frezzotti, M., Cimbelli, A. & Ferrigno, J.G. Ice-front change and iceberg behaviour along Oates and George V Coasts, Antarctica, 1912-96. *Ann. Glaciol*. **27**, 643-650 (1998).
126. Wang, X., Holland, D.M., Cheng, X. & Gong, P. Grounding and calving cycle of Mertz Ice Tongue revealed by shallow Mertz Bank. *Cryosphere* **10**, 2043-2056 (2016).
127. Diez, A. et al. Basal settings control fast flow in the Recovery/Slessor/Bailey region, East Antarctica. *Geophys. Res. Lett.* **45**, 2076-2715 (2018).
128. Lovell, A. M. Stokes, C. R & Jamieson S.S.R. Sub-decadal variations in outlet glacier terminus positions in Victoria Land, Oates Land and George V Land, East Antarctica (1972-2013), *Antarct. Sci.* **29** (5), 468-483 (2017).
129. Nakamura, K., Yamanokuchi, T., Doi, K. & Shubuya, K. Net mass balance calculations for the Shirase drainage basin, East Antarctica, using the mass budget method. *Polar Sci.* **10** (2), 111-122 (2016).
130. Kittel, C. et al. Diverging future surface mass balance between the Antarctic ice shelves and grounded ice sheet. *Cryosphere* **15**, 1215-1236 (2021).
131. Lenaerts, J.T.M., Medley, B., van den Broeke, M.R. & Wouters, B. Observing and modelling ice sheet surface mass balance. *Rev. Geophys.* **57** (2), 376-420 (2019).
132. Mottram, R. et al. What is the surface mass balance of Antarctica? An intercomparison of regional climate model estimates. *Cryosphere* **15**, 3751-3784 (2021).
133. Medley, B. & Thomas, E.R. Increased snowfall over the Antarctic Ice Sheet mitigated twentieth-century sea-level rise. *Nat. Clim. Change* **9**, 34-39 (2019).
134. Thomas, E.R. et al. Regional Antarctic snow accumulation over the past 1000 years. *Clim. Past* **13**, 1491–1513 (2017).
135. Kingslake, J., Ely, J. C., Das, I., & Bell, R.E. Widespread movement of meltwater onto and across Antarctic ice shelves. *Nature* **544** (7650), 349–352 (2017).
136. Stokes, C.R., Sanderson, J.E., Miles, B.W.L., Jamieson, S.S.R. & Leeson, A.A. Widespread distribution of supraglacial lakes around the margin of the East Antarctic Ice Sheet. *Sci. Rep.* **9**, 13823 (2019).
137. Lenaerts, J. T. M. et al. Meltwater produced by wind–albedo interaction stored in an East Antarctic ice shelf. *Nat. Clim. Change* **7**, 58-62 (2017).
138. Arthur, J.F., Stokes, C.R., Jamieson, S.S.R., Carr, J.R. & Leeson, A.A. Distribution and seasonal evolution of supraglacial lakes on Shackleton Ice Shelf, East Antarctica. *Cryosphere* **14**, 4103-4120 (2020).
139. Warner, R.C. et al. Rapid formation of an ice doline on Amery Ice Shelf, East Antarctica. *Geophys. Res. Lett.* **48**, e2020GL091095 (2021).
140. Alley, K.E., Scambos, T.A., Miller, J.Z., Long, D.G. & MacFerrin, M. Quantifying vulnerability of Antarctic ice shelves to hydrofracture using microwave scattering properties. *Remote Sens. Environ*. **210**, 297–306 (2018).
141. Lai, C.-Y. et al. Vulnerability of Antarctica's ice shelves to meltwater-driven fracture. *Nature* **584**, 574–578 (2020).
142. Kuipers Munneke, P., Ligtenberg, S. R., Van Den Broeke, M. R. & Vaughan, D. G. Firn air depletion as a precursor of Antarctic ice-shelf collapse. *J. Glaciol.* **60**, 205–214 (2014).
143. Vignon, É., Roussel, M.-L., Gorodetskaya, I.V., Genthon, C. & Berne, A. Present and future of rainfall in Antarctica. *Geophys. Res. Lett.* **48** (8), e2020GL092281 (2021).
144. Trusel, L. D. et al. Divergent trajectories of Antarctic surface melt under two twenty-first-century climate scenarios. *Nat. Geosci.* **8**, 927–932 (2015).
145. Uotila, P., Lynch, A.H., Cassano, J.J. & Cullather, R.I. Changes in Antarctic net precipitation in the 21st century based on Intergovernmental Panel on Climate Change (IPCC) model scenarios. *J. Geophys. Res*. **112**, D10107 (2007).
146. Bracegirdle, T.J. Connolley, W.M. & Turner, J. Antarctic climate change over the twenty first century. *J. Geophys. Res*. **113**, D03103 (2008).
147. Ligtenberg, S.R.M., van de Berg, W.J., van den Broeke, M.R., Rae, J.G.L. & van Meijgaard, E. Future surface mass balance of the Antarctic ice sheet and its influence on sea level change, simulated by a regional atmospheric climate model. *Clim. Dyn.* **41**, 867-884 (2013).

148. Seroussi, H. et al. ISMIP6 Antarctica: a multi-model ensemble of the Antarctic ice sheet evolution over the 21st century. *Cryosphere* **14**, 3033-3070 (2020). **Presents an intercomparison of ice flow simulations from 13 international groups and finds that East Antarctic mass change (2015-2100) varies from -6.1 cm to +8.3 cm in the simulations, with a significant increase in surface mass balance outweighing the increased ice discharge under most RCP8.5 projections.**

149. Gilbert, E. & Kittel, C. Surface melt and runoff on Antarctic ice shelves at 1.5°C, 2°C and 4°C of future warming. *Geophys. Res. Lett*. **48**, E2020GL091733 (2021).

150. IPCC, 2013: Climate Change 2013: The Physical Science Basis. Contribution of Working Group I to the Fifth Assessment Report of the Intergovernmental Panel on Climate Change [Stocker, T.F., D. Qin, G.-K. Plattner, M. Tignor, S.K. Allen, J. Boschung, A. Nauels, Y. Xia, V. Bex and P.M. Midgley (eds.)]. Cambridge University Press, Cambridge, United Kingdom and New York, NY, USA, 1535 pp.

151. IPCC, 2021: Climate Change 2021: The Physical Science Basis. Contribution of Working Group I to the Sixth Assessment Report of the Intergovernmental Panel on Climate Change [Masson-Delmotte, V., P. Zhai, A. Pirani, S.L. Connors, C. Péan, S. Berger, N. Caud, Y. Chen, L. Goldfarb, M.I. Gomis, M. Huang, K. Leitzell, E. Lonnoy, J.B.R. Matthews, T.K. Maycock, T. Waterfield, O. Yelekçi, R. Yu, and B. Zhou (eds.)]. Cambridge University Press. In Press.

152. Edwards, T.L. et al. Projected land ice contributions to 21st century sea level rise. *Nature* **593**, 74-82 (2021). **Presents statistical emulation of ISMIP6 projections, and finds East Antarctic sea level contributions of -4 to +7 cm from 2015-2100 under SSP1-2.6 and SSP2-4.5 (5-95% range), increasing to -1 to +21 cm under a risk-averse subset of the most sensitive models and inputs.**

153. Lowry, D.P., Krapp, M., Golledge, N. R. & Alevropoulos-Borrill, A. The influence of emissions scenarios on future Antarctic ice loss is unlikely to emerge this century. *Communications Earth & Environment* 2, 221 (2021).

154. Nowicki, S. et al. Experimental protocol for sea level projections from ISMIP6 stand-alone ice sheet models. *Cryosphere* **14**, 2331–2368 (2020).

155. Jourdain, N. C. et al. A protocol for calculating basal melt rates in the ISMIP6 Antarctic ice sheet projections. *Cryosphere* **14**, 3111–3134 (2020).

156. Levermann, A. et al. Projecting Antarctica's contribution to future sea level rise from basal ice shelf melt using linear response functions of 16 ice sheet models (LARMIP-2). *Earth Syst. Dynam.* **11**, 35-76 (2020).

157. Bassis, J.N., Berg, B., Crawford, A.J. & Benn, D.I. Transition to Marine Ice Cliff Instability controlled by ice thickness gradients and velocity. *Science* **372** (6548) 1342-1344 (2021).

158. Clerc, F., Minchew, B M. & Behn, M.D. Marine Ice Cliff Instability mitigated by slow removal of ice shelves. *Geophys. Res. Lett*. **46**, 12108–12116 (2019).

159. Crawford, A.J. et al. Marine ice-cliff instability modeling shows mixed-mode ice-cliff failure and yields calving rate parameterization. *Nat. Comms*. **12**, 1–9 (2021).

160. Bamber, J.L., Oppenheimer, M., Kopp, R.E., Aspinall, W.P. & Cooke, R.M. Ice sheet contributions to future sea-level rise from structured expert judgment. *Proc. Natl. Acad. Sci. U.S.A.* **116** (23) 11195-11200 (2019).

161. Hausfather, Z. & Forster, P. *Analysis: Do COP26 promises keep global warming below 2C?* Carbon Brief, 10th November 2021 (2021). Available at: https://www.carbonbrief.org/analysis-do-cop26-promises-keep-global-warming-below-2c. Last accessed 5th January 2022.

162. Ritz, C. et al. Potential sea-level rise from Antarctic ice-sheet instability constrained by observations. *Nature* **528**, 115-118 (2015).

163. Sun, S. et al. Antarctic ice sheet response to sudden and sustained ice-shelf collapse (ABUMIP). *J. Glaciol*. **66** (260), 891-904 (2020).

164. Purich, A. & England, M.H. Historical and future projected warming of Antarctic Shelf Bottom Water in CMIP6 models. *Geophys. Res. Lett*. **48** (10), e2021GL092752 (2021).

165. Bracegirdle, T.J. et al. Assessment of surface winds over the Atlantic, Indian, and Pacific Ocean sectors of the Southern Ocean in CMIP5 models: historical bias, forcing response, and state dependence. *J. Geophys. Res. Atmos*. **118**, 547–562 (2013).

166. Spence, P. et al. Rapid subsurface warming and circulation changes of Antarctic coastal waters by poleward shifting winds. *Geophys. Res. Lett*. **41**, 4601-4610 (2014).

167. Naughten, K.A. et al. Future projections of Antarctic ice shelf melting based on CMIP5 scenarios, *J. Clim.* **31**, 5243-5261 (2018).

168. Lago, V. & England, M. H. Projected slowdown of Antarctic Bottom Water formation in response to amplified meltwater contributions. *J. Clim*. **32**, 6319-6335 (2019).

169. Jourdain, N. C. et al. Ocean circulation and sea-ice thinning induced by melting ice shelves in the Amundsen Sea, *J. Geophys. Res. Oceans* **122**, 2550–2573 (2017).

170. Golledge, N.R. et al. Global environmental consequences of twenty-first-century ice-sheet melt. *Nature* **566**, 65–72 (2019).

171. England, M.H., Hutchinson, D.K., Santoso, A. & Sijp, W.P. Ice-atmosphere feedbacks dominate the response of the climate system to Drake Passage closure. J. Clim. 30, 5775-5790 (2017).
172. Purich, A., Cai, W., England, M. H. & Cowan, T. Evidence for link between modelled trends in Antarctic sea ice and underestimated westerly wind changes. *Nat. Commun.*, **7**, 10409 (2016).
173. Bintanja, R., van Oldenborgh, G.J, Drijfhout, S.S., Wouters, B. & Katsman, C. A. Important role for ocean warming and increased ice–shelf melt in Antarctic sea-ice expansion. *Nat. Geosci*. **6**, 376–379 (2013).
174. Sun, S. & Eisenman, I. Observed Antarctic sea ice expansion reproduced in a climate model after correcting biases in sea ice drift velocity. *Nat. Commun.* **12**, 1060 (2021).
175. Darelius, E., Fer, I. & Nicholls, K. W. Observed vulnerability of Filchner-Ronne ice shelf to wind-driven inflow of warm deep water, *Nat. Commun*. **7**, 12300, doi:10.1038/ncomms12300 (2016).
176. Hellmer, H., Kauker, F., Timmermann, R., Determann, J. & Rae, J. Twenty-first-century warming of a large Antarctic ice-shelf cavity by a redirected coastal current. *Nature* **485**, 225–228 (2012).
177. Paxman, G.J.G. et al. Reconstructions of Antarctic topography since the Eocene-Oligocene boundary. *Palaeogeogr. Palaeoclimatol. Palaeoecol.* **535**, 109346 (2019).
178. Albrecht, T., Winkelmann, R. & Levermann, A. Glacial-cycle simulations of the Antarctic Ice Sheet with the Parallel Ice Sheet Model (PISM)–Part 2: Parameter ensemble analysis. *Cryosphere* **14** (2), 633-656 (2020).
179. Bentley, M.J. et al. A community-based geological reconstruction of Antarctic Ice Sheet deglaciation since the Last Glacial Maximum. *Quat. Sci. Rev*. **100**, 1-9 (2014).
180. Mouginot, J., Rignot, E. & Scheuchl, B. Continent-wide, interferometric SAR phase, mapping of Antarctic ice velocity. *Geophys. Res. Lett*. **46** (16), 9710-9718 (2019).
181. Zachos, J., Pagani, M., Sloan, L., Thomas, E. & Billups, K. Trends, rhythms, and aberrations in global climate 65 Ma to present. *Science* **292** (5517), 686-693 (2001).
182. Mazloff, M., Heimbach, P. & Wunsch, C. An Eddy-Permitting Southern Ocean State Estimate. *J. Phys. Oceanogr.* **40**, 880-899 (2010).
183. NOAA National Geophysical Data Center: 2-minute Gridded Global Relief Data (ETOPO2) v2. NOAA National Centers for Environmental Information. https://doi.org/10.7289/V5J1012Q (2006).

Acknowledgements:

CRS, BWJM and SSRJ acknowledge funding from the Natural Environment Research Council (NE/R000824/1). MAK, NJA, and MHE are supported by the Australian Research Council Special Research Initiative, Australian Centre for Excellence in Antarctic Science (Project Number SR200100008), and RSJ is supported by the Special Research Initiative, Securing Antarctica's Environmental Future (SR200100005). NJA (FT160100029), MHE (DP190100494, LP200100406) and RSJ (DE210101923) also acknowledge funding from the Australian Research Council. MHE and MAK also acknowledge support from the Centre for Southern Hemisphere Oceans Research (CSHOR), a joint research centre between QNLM, CSIRO, UNSW and UTAS. AF was supported by the Australian Antarctic Program Partnership through funding from the Australian Government as part of the Antarctic Science Collaboration Initiative. TLE was supported by the UK Natural Environment Research Council (NE/T007443/1) and by the European Union's Horizon 2020 research and innovation programme under grant agreement No 869304, PROTECT contribution number 36. JTML acknowledges support from the National Aeronautics and Space Administration (NASA), award #80NSSC20K1123. MHE and AF thank Steve Rintoul for discussions on ocean data coverage around East Antarctica. TLE thanks Gregory Garner and Robert Kopp for help with

IPCC (2021) datasets. We thank the Editor, Michael White, together with Johann Klages, Ed Gasson and three anonymous referees, who provided constructive reviews of the manuscript.

Figure Captions:

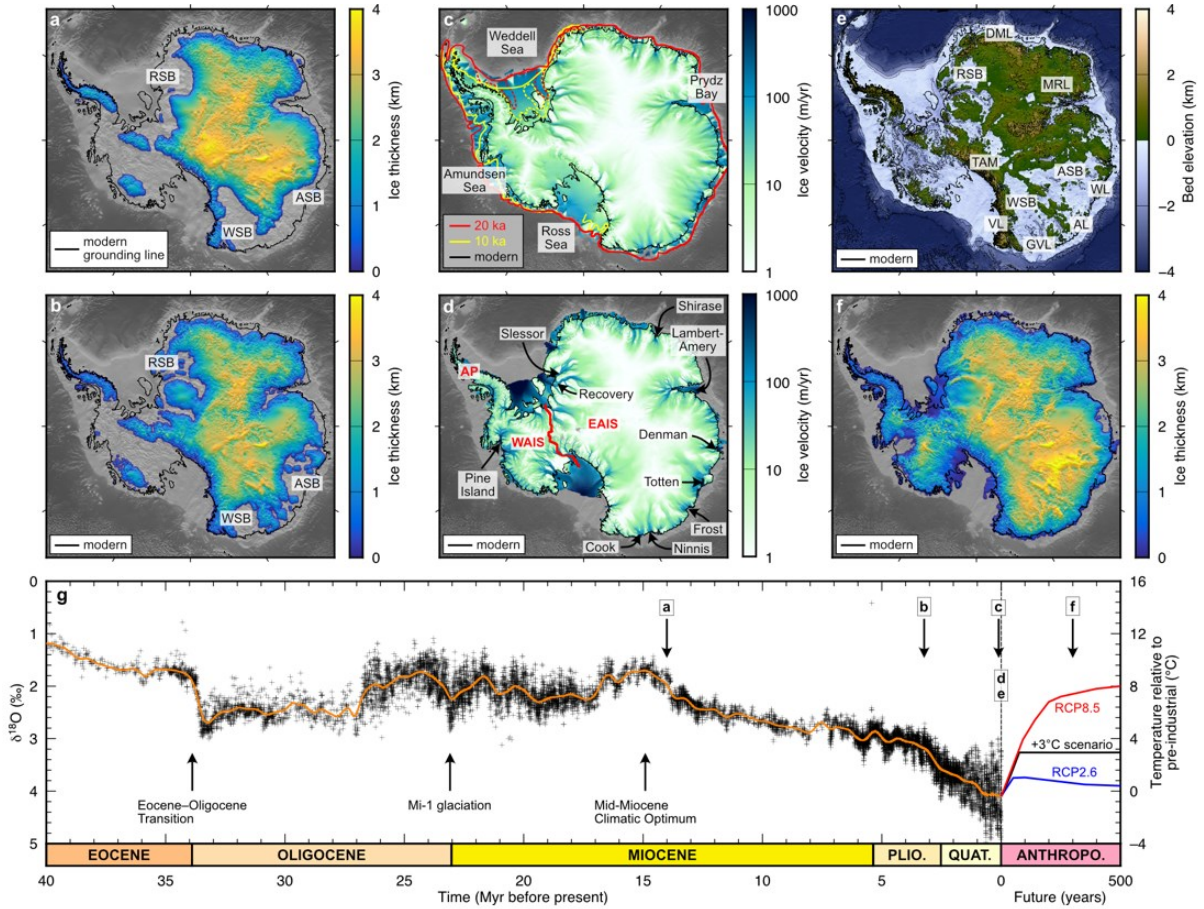

Figure 1: Grounding line extent and characteristics of the East Antarctic Ice Sheet (EAIS) at selected times in the past, present and future. (a) Modelled ice thickness during the Mid-Miocene[57] and reconstructed Mid-Miocene palaeotopography[177] in greyscale, showing deglaciation of West Antarctica and East Antarctica's three major subglacial basins: the Recovery (RSB), Wilkes (WSB) and Aurora (ASB). **(b) Modelled ice thickness during a warm mid-Pliocene** interglacial with hydrofracturing and ice-cliff calving physics enabled[46] and reconstructed mid-Pliocene palaeotopography[177] in greyscale. **(c) Modelled Last Glacial Maximum (20 ka) ice surface velocities** from a Parallel Ice Sheet Model ensemble best-fit reference simulation[178] and RAISED consortium grounding lines at 20 ka (red) and 10 ka (yellow) inferred from empirical data[179] (dashed lines depict a RAISED scenario in the Weddell Sea that is now considered less likely[94]). **(d) Present-day ice surface velocities** derived from interferometric SAR phase mapping[180], with selected outlet glaciers labelled together with EAIS, West Antarctic Ice Sheet (WAIS) and Antarctic Peninsula (AP). Note that we use the standard definition of the EAIS as Antarctic drainage basin numbers 2-17 (e.g. refs [1, 24]). **(e) Present-day Antarctic bed topography and Southern Ocean bathymetry** from BedMachine[10] (AL = Adélie Land; DML = Dronning Maud Land; GVL = George V Land; MRL = Mac. Robertson Land; TAM = Transantarctic Mountains; WL = Wilkes Land; VL = Victoria Land). **(f) Modelled ice thickness at 2300 under a 3°C warming** scenario[46]. **(g) Global benthic oxygen isotope curve through the Cenozoic**[181] with a 1 Myr-smoothed trend line (orange). The projected temperature of the end-member RCP2.6 (blue) and RCP8.5 (red) future emissions scenarios are displayed to the year 2500. The ice configurations shown in panels a–f are labelled along the timescale.

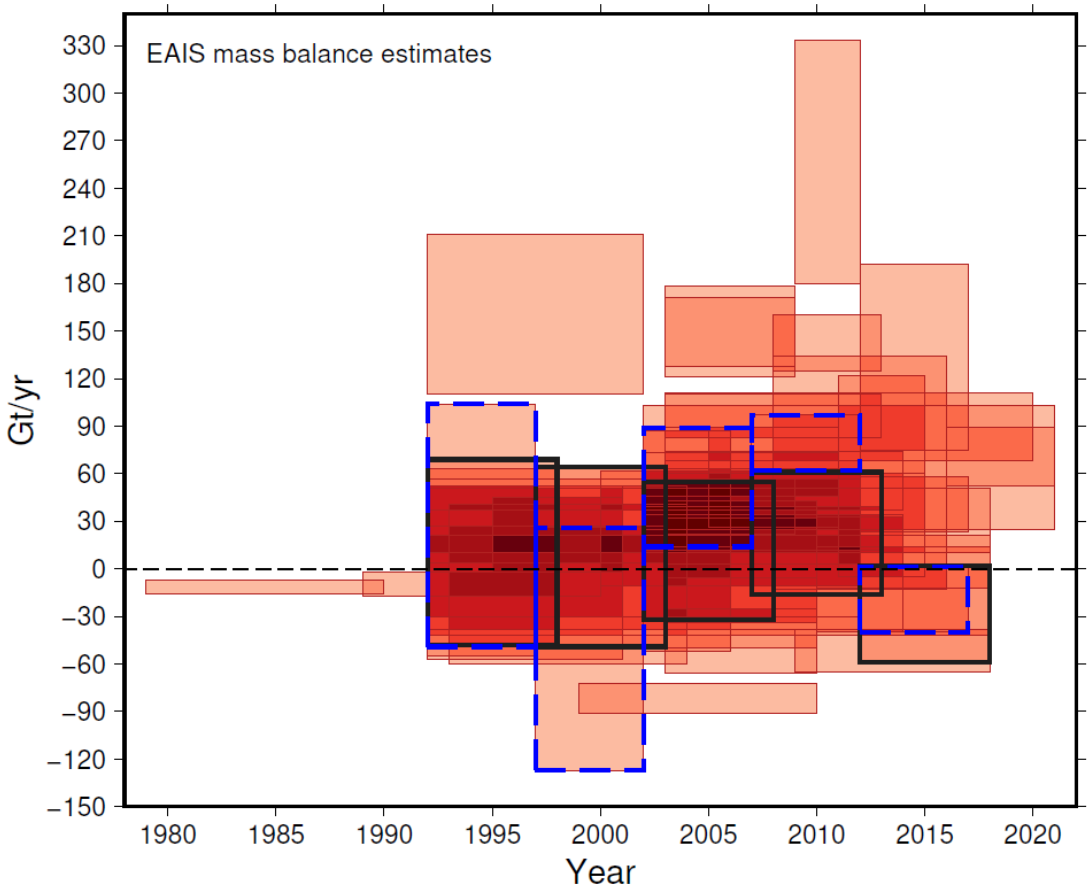

Figure 2: Published estimates of the net mass balance of the East Antarctic Ice Sheet. Each box represents a single estimate of net mass balance with overlapping estimates indicated by darker shading. The horizontal extent of each box represents the survey period. Most studies provide annual data plotted from 1st January to 31st December for any given year. The vertical extent of each box represents the stated uncertainties. Survey areas may vary slightly between different studies, but only those that partition the net mass balance of the EAIS or a large part thereof are included (see Source Data file for numeric values and references). Two recent attempts to reconcile data from multiple methods are highlighted in black[1] and dashed blue[2] lines.

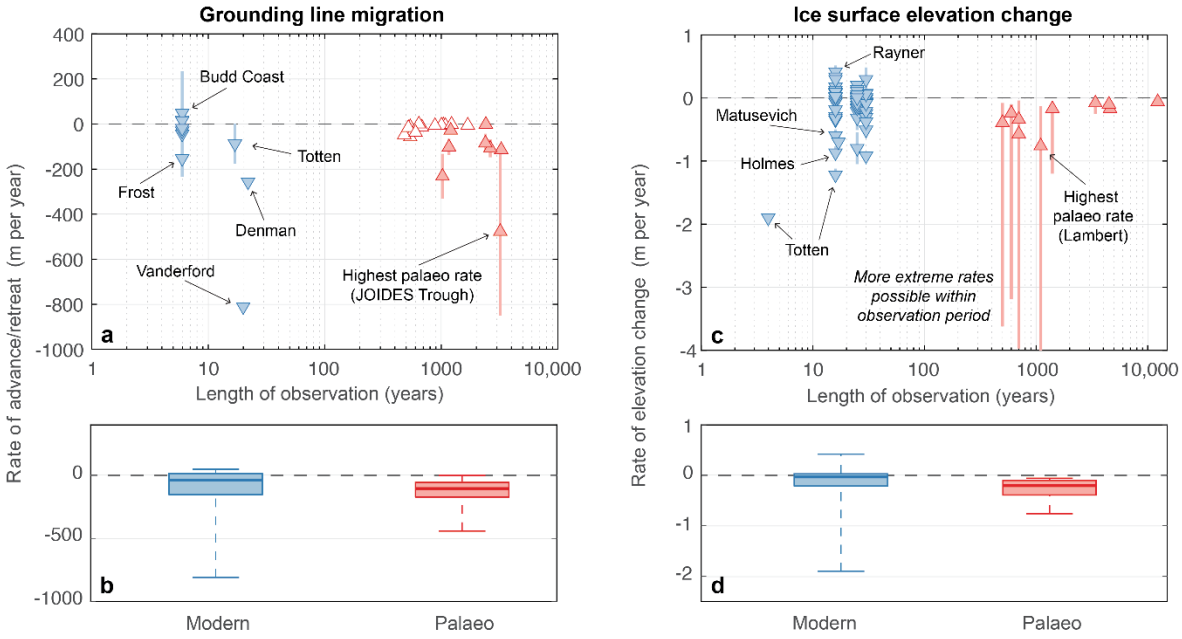

Figure 3: Comparison between published estimates of modern and palaeo (last deglaciation) rates of grounding line migration and ice surface elevation change. (a) Rates of grounding line advance (positive) and retreat (negative) for modern (blue) and palaeo (red) estimates plotted against length of observations. For modern estimates, the triangle marker denotes the mean and the vertical line extends to the maximum possible advance or retreat value quoted in the study. For palaeo estimates, the triangle represents the mean and the vertical line represents the minimum-maximum range, where available. White triangles are minimum palaeo estimates based on the grounding line reaching its present-day position zero years ago. **(b) Box and whisker plots for the range of modern and palaeo mean estimates of grounding line migration.** The median and interquartile range is represented by the horizontal line and the box extent, respectively, while the range is shown by the vertical dashed line. **(c) Rates of ice sheet thickening (positive) and thinning (negative) for modern (blue) and palaeo (red) estimates** plotted against the length of observations. Modern rates from selected East Antarctic outlet glaciers are mean rates extracted from a 20 km x 20 km box immediately up-ice of the grounding line from three recently published altimetry studies[5-7]. Triangle markers and vertical lines represent the mean and published uncertainty range for the modern estimates, and the median and 95% confidence range for the palaeo estimates. **(d) Box and whisker plots for the range of modern (mean) and palaeo (median) estimates of ice surface elevation change** (as in 'c'). See Source Data for numeric values, uncertainties and references. Note that all palaeo-estimates are time-averaged rates for the period of observation and actual rates could have been lower/higher within the period.

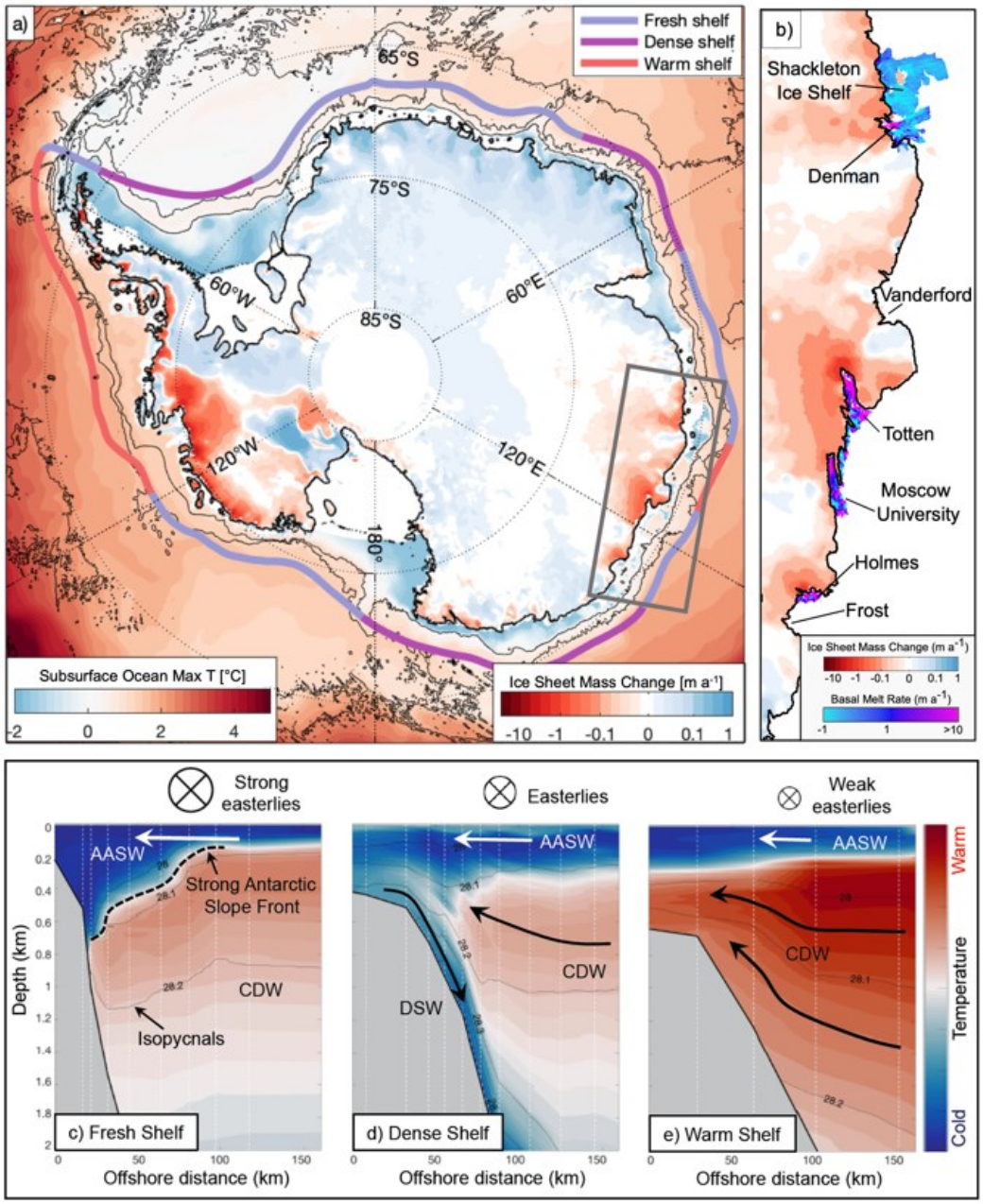

Figure 4: Modern oceanic conditions and characteristic shelf/slope regimes around East Antarctica in relation to recent ice sheet mass changes. (a) Oceanic colours show the 2005-2010 mean subsurface ocean potential temperature maximum from the Southern Ocean State Estimate[182]. Black lines indicate isobaths from ETOPO2v2 (ref. [183]), contoured every 2000 m from the 1000-m isobath; thick black line is the Antarctic continental coast. The thick coloured line parallel to the coast differentiates the three main oceanic shelf regimes (fresh shelf, dense shelf, warm shelf: from ref. [110]).Continental colours represent data from a recent altimetry study[7] of ice sheet elevation change (2003-2019), corrected for firn air content to reflect mass change. **(b) Firn Air Content-corrected ice elevation change in Wilkes Land**, as in (a) with location shown, together with time-averaged ice shelf basal melt rates (2010-2018) from ref. [116]. Note the correspondence between mass loss and high basal melt rates. **(c, d, e) Schematic latitude-depth transects indicating typical winds, subsurface ocean circulation, temperature and density structure in a (c) fresh shelf, (d) dense shelf and (e) warm shelf regime** (modified from ref. [110]). Colours represent temperature and black contours isopycnals of neutral density, with the bold black dashed line in (c) indicating the sharp density gradient across the Antarctic Slope Front. Cross-slope circulation is shown schematically with black and white arrows, and wind direction and strength by arrow tails going into the page. Water masses shown include Antarctic Surface Water (AASW), Circumpolar Deep Water (CDW), and Dense Shelf Water (DSW, also referred to High Salinity Shelf Water in some sectors).

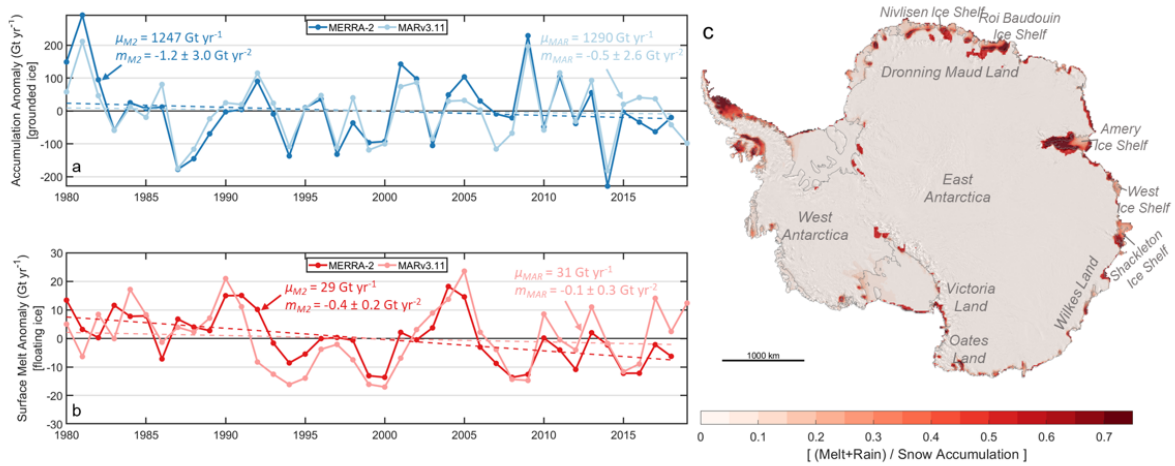

Figure 5: Recent temporal and spatial trends in Antarctic snow accumulation and surface melt. (a) Annual snow accumulation rates integrated over the entire grounded EAIS expressed as an anomaly from the 39-year mean (1980–2018; μ_{M2} = 1,247 Gt yr^{-1}; μ_{MAR} = 1,290 Gt yr^{-1}; from ref. [7] and [130], respectively). The 1980–2018 trends are displayed as dashed lines. (**b**) **As in (a) but for annual surface melt rates over floating ice** only (μ_{M2} = 29 Gt yr^{-1}; μ_{MAR} = 31 Gt yr^{-1}). **(c) The average liquid-to-solid ratio from MERRA-2[7] and MAR[130] over both the WAIS and EAIS** (grounded and floating), where values approaching zero reflect areas of a thick, porous firn column capable of storing liquid water and those approaching one reflect areas with little to no pore space. See Source Data file for numeric values.

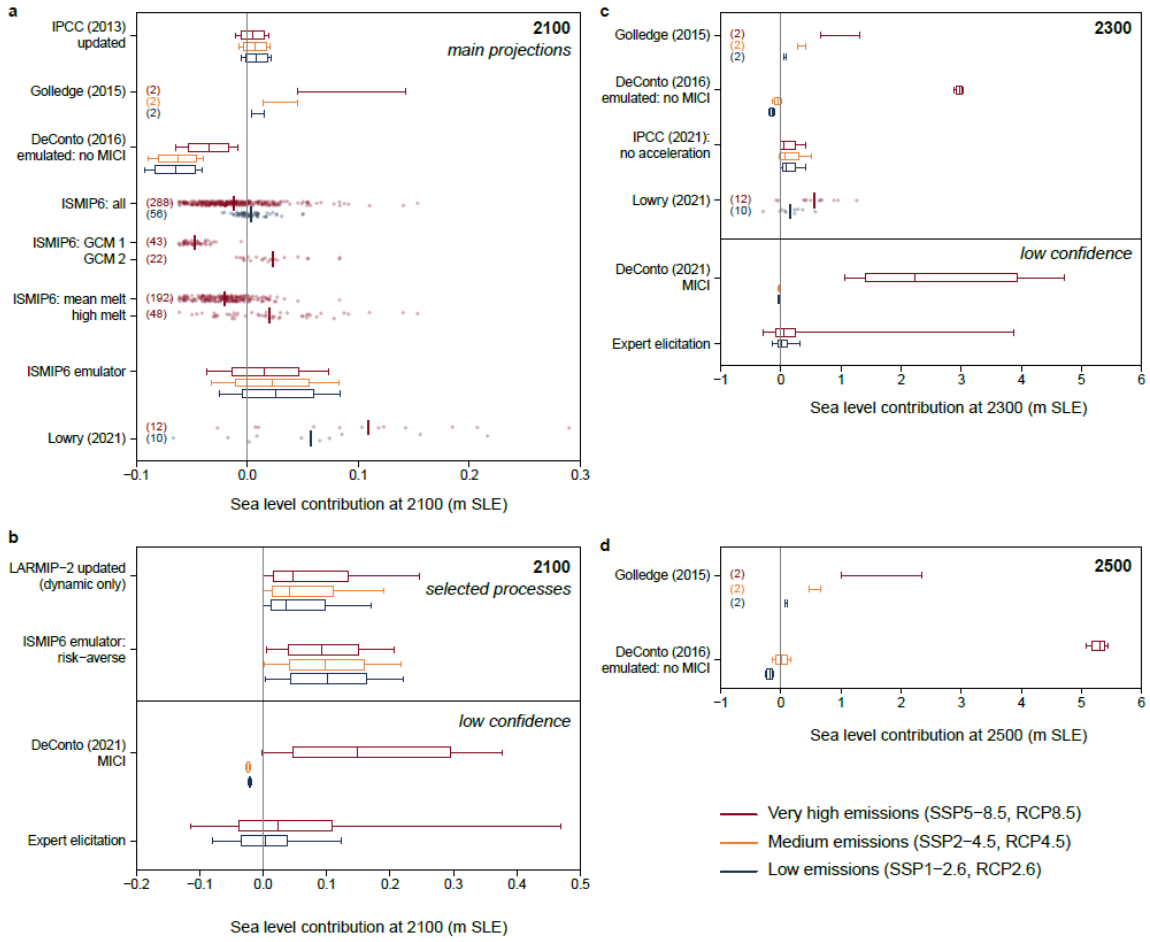

Figure 6: Projected sea level contribution from the East Antarctic Ice Sheet at 2100, 2300 and 2500 under very high, medium and low emissions scenarios. **(a) Projections at 2100** from: IPCC (2013) method, re-estimated for IPCC (2021)[151]; ref. [43]; emulated estimate of ref. [44] without Marine Ice Cliff Instability (MICI) mechanism using method of ref.[86]; ISMIP6 multi-model ensemble[25,148,152]; sub-sets of ISMIP6 ensemble using climate forcing from two different Global Climate Models (CCSM4 and HadGEM2-ES), with mean sub-ice shelf melting; subsets of ISMIP6 ensemble using mean versus high sub-ice shelf melting treatment; emulated ISMIP6 projections[152] re-estimated for IPCC (2021)[151], including the addition of 0.09 mm/yr response to pre-2015 climate change; ref.[153], subtracting control simulation and adding the same pre-2015 response. **(b) Projections at 2100 for selected processes and 'low confidence' projections** from: LARMIP-2 dynamic-only contribution[156] re-estimated for IPCC (2021)[151]; emulated ISMIP6 'risk-averse' projections[152] using a high sea-level subset of models and parameter values, with +1.1 cm contribution added to approximate re-estimation for IPCC (2021)[151]; with MICI enabled[46]; expert elicitation[160]. **(c) Projections at 2300** from: ref. [43]; emulated estimate of ref. [44] without MICI, using method of ref. [86]; p-box of IPCC (2013) method[150] and dynamic-only contribution[156], extrapolated beyond 2100 with fixed rate mass loss from IPCC (2021)[151]; ref. [153], subtracting control simulation; with MICI[46]; expert elicitation[160]. **(d) Projections at 2500** from: ref. [43]; emulated estimate of ref. [44] without MICI using method of ref. [86]. Small dots show individual simulations, with short vertical lines showing ensemble means; whiskers without box show range of two simulations. Numbers of simulations are given in brackets. Central line and whiskers show median and 5-95% range; box shows 16%-84% for ref. [44] or 17-83% otherwise. All relative to 1995-2014 baseline[151] except for refs [43,44], relative to 2000; ISMIP6 ensemble, relative to 2015; and ref. [153] for 2105 and 2301, relative to 2025. All use identical climate forcing under Shared Socioeconomic Pathways (SSPs) from IPCC (2021)[151], except for refs [43,44,46], forced with regional climate model (RegCM3) under Representative Concentration Pathways (RCPs); ISMIP6 simulations, forced with various global climate models under RCPs and SSPs; IPCC (2021) no acceleration[151], which has no climate dependence beyond 2100; and expert elicitation, where warming scenarios are interpreted as SSPs following ref.[151]. See Source Data file for numeric values.